Water Resources Research

RESEARCH ARTICLE
10.1029/2018WR024107

Deposition Potential and Flow-Response Dynamics of Emergent Sandbars in a Braided River

Jason S. Alexander[1], Brandon McElroy[1], Snehalata Huzurbazar[2], Caroline Elliott[3], and Marissa L. Murr[1]

[1]Department of Geology and Geophysics, University of Wyoming, Laramie, WY, USA, [2]Department of Biostatistics, West Virginia University, Morgantown, WV, USA, [3]U.S. Geological Survey-Columbia Environmental Research Center, Columbia, MO, USA

Key Points:
- Potential to deposit emergent sandbars is a positive function of Parker (1976) stability criteria and a gradient in sediment transport mode
- Emergent sandbar top-surface height grows linearly with formative flood magnitude at a rate that lags growth of formative flood stage
- Emergent sandbar persistence is largely dependent on sandbar starting size, which itself is dependent on formative flood magnitude

Supporting Information:
- Supporting Information S1
- Table S1

Correspondence to:
J. S. Alexander,
js.alexand@gmail.com

Citation:
Alexander, J. S., McElroy, B., Huzurbazar, S., Elliott, C., & Murr, M. L. (2020). Deposition potential and flow-response dynamics of emergent sandbars in a braided river. *Water Resources Research*, *56*, e2018WR024107. https://doi.org/10.1029/2018WR024107

Received 21 SEP 2018
Accepted 18 NOV 2019
Accepted article online 23 NOV 2019

Abstract Sandbars are ubiquitous in sandy-braided rivers throughout the world. In the Great Plains of the United States, recovery and expansion of emergent sandbar habitat (ESH) has been a priority in lowland rivers where the natural extent of sandbars has been degraded. Recovery efforts are aimed at protection of populations of the interior least tern (*Sterna antillarum*) and piping plover (*Charadrius melodus*). But quantitative observations of deposition and erosion dynamics of populations of sandbars across long segments of rivers are rare. We present a three-part case study which used Bayesian regression models to examine relations between hydrology, channel morphology, and ESH responses in the Platte River, eastern Nebraska. Logistic regression indicates presence of ESH is positively related to the Parker, (1976, https://doi.org/10.1017/S0022112076000748) stability criterion and a gradient in sediment transport mode, and negatively related to presence of vegetation. Hierarchical linear regression modeling shows direct coupling between sandbar top-surface height and formative flood magnitude, but the gap between formative flood stage and sandbar top-surface increases with increasing discharge. Finally, linear regression modeling of sandbar erosion demonstrates rates of ESH erosion are on the order of 10^{-1} ha/day during high-flow periods and 10^{-2} during low-flow periods, but sandbar persistence is largely a function of sandbar starting size. The collective observations highlight the importance of large floods (>3-year recurrence) in creating very large sandbars that persist as high-quality ESH over periods of years whereas lower-magnitude, more-frequent flood events create lower-quality ESH that typically does not persist into the following nesting season.

1. Introduction

Sandbars (macroforms) are ubiquitous in sandy-braided rivers throughout the world (Brice, 1964; Cant & Walker, 1978; Coleman, 1969; Collinson, 1970; Crowley, 1983; Santos & Stevaux, 2000; Smith, 1971). In the Great Plains of the United States, recovery and expansion of emergent sandbar habitat (ESH), broadly defined here as areas of labile, unvegetated riverine sandbars (Council, 2010), has been a priority in lowland rivers where the natural extent has been degraded due to human modification of hydrologic and sediment regimes and/or channel planform (Council, 2002, 2004; Friedman et al., 1998; Johnson, 1994). Recovery of ESH has been aimed at protection of the interior least tern (*Sterna antillarum*) and piping plover (*Charadrius melodus*), federally listed bird species which use ESH as nesting and foraging habitat (Catlin et al., 2014; Driesen, 1996; Price & Martz, 2007). Additionally, sandbars are recognized as aquatic and terrestrial-transition zone features important to many species using the river corridor (Tracy-Smith et al., 2012). Sandbars also form the foundation for establishment and growth of riparian plants (Dixon, 2003; Johnson, 1994). The importance of emergent sandbars has been recognized in large riverine ecosystems across the globe including the Mekong (Duckworth et al., 1998; Evans, 2001; Schwilk & Claassen, 2012), the Paraná (Gimenes & Anjos, 2004), the Ganges (Dilawar & Sharma, 2016; Sundar, 2004; Whitaker, 2007), and the Amazon (Rosenberg, 1990; Valenzuela, 2001).

Despite the importance of ESH to river ecology and management, quantitative observations of the deposition and erosion dynamics of populations of sandbars across long segments of river are relatively rare. Geologists and geomorphologists have published observations of the migration, deposition, emergence, and erosion of sandbars, but these observations are often limited to one or two sandbars in isolated reaches, and have quantitative descriptions aimed at interpreting the geologic record (e.g., Ashworth et al., 2000; Parker et al., 2013;

Smith, 1971). Recent advances in numerical morphodynamic models produce realistic channel and floodplain patterns for a variety of channel types (Nicholas, 2013; Schuurman et al., 2013), but obtaining model boundary conditions over long river segments is impractical within typical management efforts. Separately, studies focused on river and species management have measured physical characteristics of ESH over larger spatial scales, and demonstrated their importance to riverine ecosystems, but these characteristics have not been dynamically linked to fluvial processes. Consequently, models of ESH habitat quality and abundance have treated sandbars as either static, long-lived (>5 years) habitat features subject to changes in river stage (Tracy-Smith et al., 2012) or modeled ESH dynamics using growth and decay functions as heuristic models (Buenau et al., 2014). In short, case studies are needed to improve understanding of ESH dynamics across the extensive scales (>10 km) that moderate-to-large rivers are managed.

We present a case study of emergent sandbar deposition and erosion dynamics in the Platte River in eastern Nebraska, a large braided river at the eastern margin of the Great Plains, United States. The study is presented as three main components: (1) physical controls on the potential to deposit ESH, (2) response of ESH top-surface elevation to river discharge, and (3) ESH erosion rates and population persistence. The three components represent a collective understanding of populations of sandbars acting as ESH in a braided river with a mostly natural flow and sediment regime. The first component addresses the bulk physical conditions influencing locations of deposition of ESH. The second component demonstrates coupling between river discharge and sandbar top-surface height, a primary determinant of bird nest inundation (Lott et al., 2013; Smith & Renken, 1993). The last component documents natural rates and processes of erosion of populations of sandbars relative to flow magnitude and starting size. While adding to geologic and geomorphic understanding of macroform sandbars, our findings are most directly applicable to management, conservation, and restoration of braided river ecosystems.

1.1. Physical Setting of the Platte River Study Area

The Platte River is a large tributary to the Missouri River draining approximately 222,800 km^2, including large areas of the Rocky Mountains, Great Plains, and Eastern Lowland physiographic provinces in Colorado, Wyoming, and Nebraska (Figure 1; Eschner et al., 1983; Fenneman, 1928). The Platte River begins at the confluence of the North and South Platte Rivers near the city of North Platte, Nebraska, and can be divided into two main segments, a snowmelt-runoff dominated segment upstream from the Loup River confluence (locally referred to as the "central Platte River") and a groundwater seepage/runoff-dominated segment downstream from the Loup River confluence (locally referred to as the "lower Platte River" [LPR]; Bentall & Schaffer, 1979).

The morphology, hydrology, and sediment regime of the central Platte River are substantially altered by upstream dams and diversions (Council, 2004; Eschner et al., 1983; Williams, 1978). The LPR is less directly altered and has been mostly stable since the middle twentieth century, likely due to large flow and sediment contributions from the mostly free-flowing Loup and Elkhorn River systems (Ginting et al., 2007; Joeckel & Henebry, 2008; U.S. Army Corps of Engineers, 2014). The most obvious human alteration to the flow regime of the LPR is a diel cycle of a maximum of about 100 m^3 s^{-1} from the outfall of an off-channel hydroelectric facility which joins the LPR 3 km downstream from the Loup River (Loup River power outfall).

Our study area is the 163-km segment of the LPR downstream from the Loup River power outfall to the beginning of the backwater zone approximately 6 km upstream of the confluence with the Missouri River (Figure 1). Median bed material grain size (D_{50}) in the LPR ranges from 0.30 to 0.50 mm (Kinzel & Runge, 2010; U.S. Army Corps of Engineers, 2014) and hydraulic properties change at confluences with the Elkhorn River and Salt Creek, creating three hydrologic subsegments (Figure 1). From 1990 to 2014 mean annual floods in the subsegments were 790, 1,300, and 1,470 m^3 s^{-1}, respectively. Bed slope is 0.091% until the Elkhorn River confluence, where it declines to 0.075% (Bentall, 1991). Herein, we refer to the segment upstream from the Elkhorn River "Geomorphic Segment 1" (GS1) and the downstream segment "Geomorphic Segment 2" (GS2) (Figure 1). Mean active channel width in both segments is approximately 500 m, but the wider alluvial valley of GS1 is coincident with more abundant islands than GS2 (Elliott et al., 2009). Total channel width (including vegetated islands) in GS1 ranges from 200 to 1,400 m compared to a range of 200 to 850 m in GS2. Channel sinuosity is low in both segments, generally not exceeding 1.10.

1.2. Sandbars: Theory and Process

The occurrence of sandbars is a consequence of flow-depth scale turbulence, which grows through a morphodynamic feedback between bed topography and reach-scale channel hydraulics (Church & Ferguson,

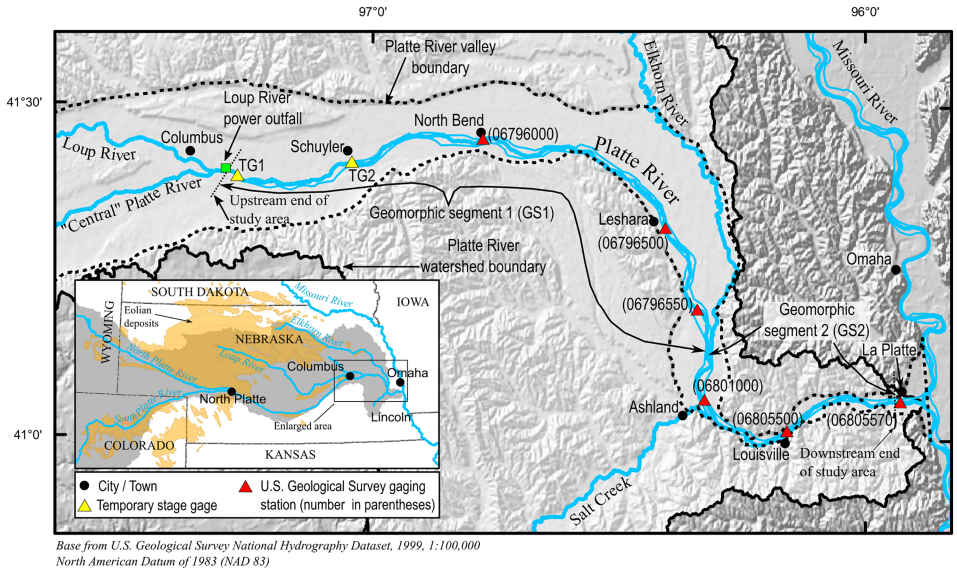

Base from U.S. Geological Survey National Hydrography Dataset, 1999, 1:100,000
North American Datum of 1983 (NAD 83)

Figure 1. Location map of the lower Platte River study area, major tributaries and subbasins, and locations of U.S. Geological Survey gaging stations and temporary stage gages.

2015; Kleinhans, 2010). Sandbar formation requires channel aspect ratios (wetted width/mean channel depth) more than about 9, and braiding requires aspect ratios of more than 60 (Rhoads & Welford, 1991, and references therein). While sandbar formation has been observed to cause channel expansion (Ashmore, 1996; Ashworth et al., 2000; Leopold & Wolman, 1957), where bank erosion rates are low relative to rates of sandbar formation, channel morphology may force sandbar formation through bank curvature, width expansions, and contractions (Cant & Walker, 1978; Jiongxin, 1997; Repetto et al., 2002; Struiksma et al., 1985; Szupiany et al., 2012; Wu & Yeh, 2005; Wu et al., 2011).

Heights and lengths of sandbars scale with flow depths and widths, respectively (Bridge, 1993). When discharge increases, sandbars grow vertically through bedform climbing on the sandbar stoss, with the limit being the water surface (Ashworth et al., 2000; Crowley, 1983; Mohrig, 1994; Sambrook Smith et al., 2009). When flow stage recedes, sandbars stall and emerge (emergent sandbars), causing flow division, producing a braided flow pattern (Brice, 1964; Sarma, 2005). Emergent sandbars have been variously referred to as “islands,” “sand islands,” and “sand flats” (Brice, 1964; Buchanan & Schumm, 1990; Collinson, 1970; Cant & Walker, 1978). The term “compound bars” has also been used in reference to amalgams of emergent sandbars (Bridge, 1993). Sandbars in the LPR have been extensively described by Smith (1971) and Crowley (1983) and are dominated by transverse bars, although other types are present. Herein, we use the general term “sandbar” to include the host of emergent sandbars in the LPR, which may have little gross resemblance to actively migrating transverse sandbars (Figure 2).

2. Materials and Methods

Two primary data sets were used for the three-part case study. For the first part, remotely sensed data were used to extract a binary response variable (m_i, presence/absence of extensive ESH) along evenly spaced reaches of river. Because the response variable was binary, logistic regression was used to assess the relative influence of physical controls on m_i. The second and third parts used data collected from field surveys to characterize ESH vertical growth and erosion dynamics; linear regression models were used for these analyses because the response variables were continuous. Bayesian methods were used for all modeling and analysis because we were most interested in probability distributions for parameters, beyond obtaining point estimates. Below, the methods for each study component are presented in two parts: (1) data presentation and (2) statistical models. The supporting information has additional method details. Data supporting these analyses can be found in Alexander and Densmore (2019).

2.1. Methods Part 1: Emergent Sandbar Deposition Potential

Four explanatory variables were hypothesized as contributing to the binary response variable (m_i), the presence\absence of extensive ESH in a reach of river: (1) Parker (1976) stability criterion (ε^*), a bar-theory

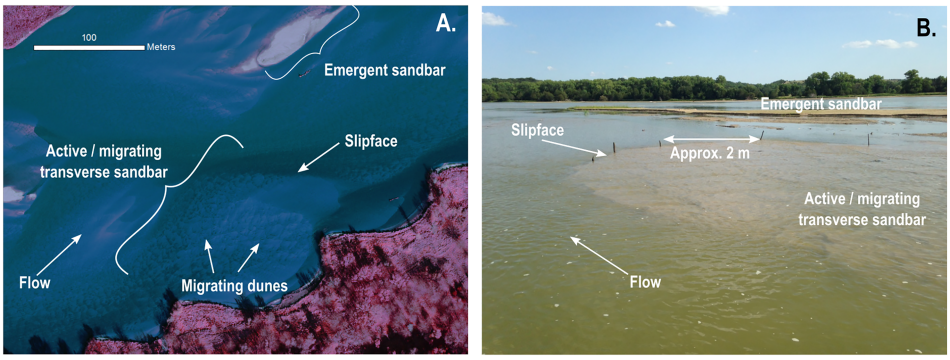

Figure 2. Images depicting active, migrating sandbars and emergent sandbars considered emergent sandbar habitat. (a) False-color aerial image of Platte River in eastern Nebraska (U.S. Army Corps of Engineers, 2013). (b) Ground-level photo of actively migrating linguoid sandbar and emergent sandbar in the Niobrara River of northern Nebraska; the emergent sandbar is approximately 40 m long.

indicator of channel tendency toward single or multiple threads; (2) fraction of reach covered by vegetation (V^*), since vegetation is a biogeomorphic agent important in the transition from multithread to single-thread channels (Johnson, 1994; Tal & Paola, 2007); (3) planform channel centerline curvature (C^*), a driver of secondary flow and sandbar formation (Dietrich & Smith, 1983); and (4) longitudinal gradient in sediment transport mode (P^*), intended to capture channel expansion/contraction effects on sandbar formation (Repetto et al., 2002; Szupiany et al., 2012). We use the term "deposition potential" synonymously in reference to probability of occurrence of ESH.

2.1.1. Data

Supervised classification of digital-aerial images was the primary data extraction method. Additional data were obtained from a LiDAR-derived digital elevation model and publicly available hydrologic and sediment data. Three sets of images were classified representing emergent sandbar conditions after small, moderate, and large floods (Table 1). Image classification resulted in three final classes: (1) water (submerged river bed); (2) emergent sand; and (3) vegetation (Figure 3a). The area of each class was extracted from 500-m-long polygons (extraction polygons), defined by upstream and downstream boundaries perpendicular to the centerline coordinate system of Elliott et al. (2009) and bankline boundaries digitized for this study. High-flow conditions during image acquisition along the downstream-most 40 km of the 2010 images caused submergence of sandbars. For that segment, in that year, the April 2011 sandbar survey of Alexander et al. (2013) was used to quantify the spatial distribution of emergent sand.

The Parker (1976) stability criterion was calculated using the following form:

$$\varepsilon^* = \frac{\zeta_i \sqrt{g h_i W_i^4}}{\bar{\bar{Q}}_i} \tag{1}$$

Table 1
Dates, Sources, and Hydrologic Conditions of Aerial Imagery Used for Image Classification to Extract Emergent Sandbar Conditions

						Flow range (U/S)[a]		Flow range (D/S)[b]	
Year	Source[c]	Image acquisition date range[d]	Bands	Pixel resolution (m)	Spring flood R.I.[a]	min (m^3/s)	max (m^3/s)	min (m^3/s)	max (m^3/s)
2006	USDA-NAIP	18–30 July	3	2	1.05–1.17	16	26	8	21
2010	USDA-NAIP	16 June to 12 August	3	1	6.8–21	151	2,800	113	1,180
2014	USDA-NAIP	7–21 September	3	1	1.44–3.8	47	210	157	637

[a]USDA-NAIP (U.S. Department of Agriculture-National Aerial Information Program). [b]Images were taken over a range of dates; image classification used a mosaic of these images. [c]R.I. (recurrence interval) ranges calculated using simple plotting position for three USGS streamflow gages (06796000, 06801000, and 06805500), using the data from water years 1990 to 2014. A water year is defined as starting on 1 October of previous calendar year. [d] Flow ranges shown for USGS Streamflow Gages 06796000 and 06805500, representing the upstream-most (U/S) and downstream-most (D/S) flow conditions, respectively. Ranges shown indicate known ranges during dates of photo acquisition. Our visual assessment indicated that the highest discharges shown for 2010, which submerged many of the emergent sandbars, were only occurring in the downstream-most 40 km of the study area. For that reach the emergent sandbar survey data of Alexander et al. (2013) were used to populate the locations and spatial extent of emergent sandbars.

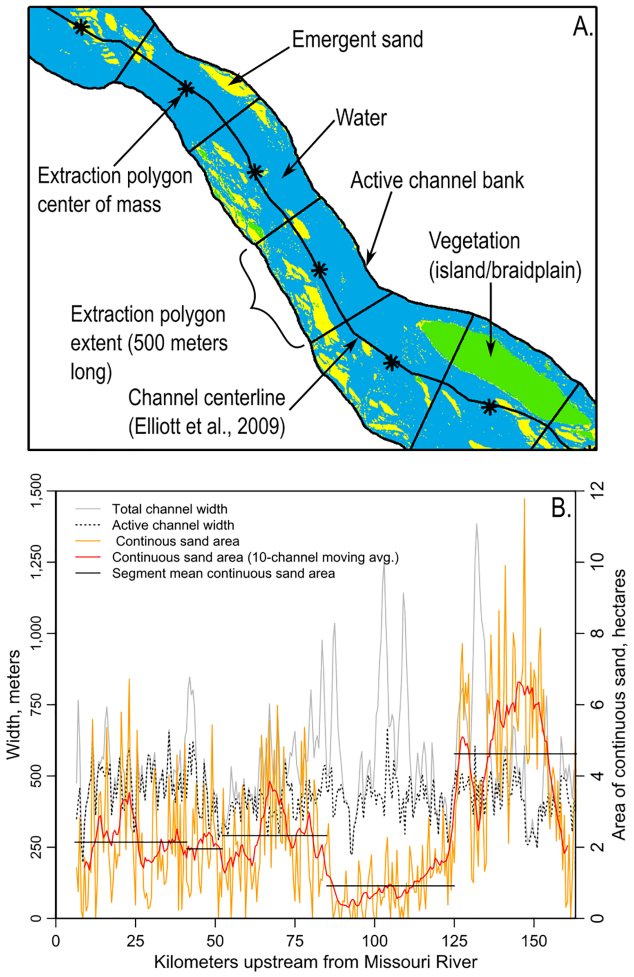

Figure 3. (a) Example of classified image used to inform logistic regression analysis, including 0.5-km-long extraction polygons, polygon centers, channel centerline and channel boundaries. Note the slightly sinuous channel with substantial along-stream changes in channel width. (b) Longitudinal characteristics extracted from supervised classification of the 2014, USDA image, including segment mean sandbar areas used to define threshold of exceedance for the logistic regression response variable (m_i).

where ζ_i is longitudinal channel slope (dimensionless), g is the gravitational constant in units of meters per square second, and h_i and W_i are, respectively, the mean channel depth and wetted width in units of meters for some annual peak discharge ($\bar{\bar{Q}}_i$) in polygon i in units of cubic meters per second. The method of Wright and Parker (2004) was used to estimate h_i, and wetted width was estimated using continuity:

$$W_i = \frac{A_{a_i}}{500 \text{ m}}, \tag{2}$$

where A_{a_i} is the active (nonvegetated) area of polygon i in units of square meters. Fraction of polygon as vegetation was expressed as follows:

$$V^* = \frac{A_{v_i}}{A_{t_i}}, \tag{3}$$

where A_{v_i} and A_{t_i} are vegetated area and total area of polygon i, respectively. Channel curvature was defined as follows:

$$C^* = \frac{S_{i_{+2}} - S_{i_{-2}}}{\sqrt{(X_{i_{-2}} - X_{i_{+2}})^2 + (Y_{i_{-2}} - Y_{i_{+2}})^2}}, \tag{4}$$

where S_i, X_i, and Y_i are, respectively, the channel centerline, UTM-easting, and UTM-northing coordinates of extraction polygon centers of mass in units of meters, and ± 2 is the index for two polygons upstream (+) or downstream (−) of polygon i. The along-stream gradient in sediment transport mode was calculated as follows:

$$P^* = \frac{P_{i_{+2}} - P_i}{S_{i_{+2}} - S_i}, \tag{5}$$

where P_i is the Rouse number (dimensionless) computed using the equation of Rouse (1939). Figure 4 shows the distributions of the explanatory variables used in the logistic regression for each image year and the two geomorphic segments.

River stage is a primary control on the amount of sand exposed in aerial images. Figure 3b, for example, demonstrates spatial variability of area classified as continuous exposed sand caused by spatial variability in stage from hydrocycling (hydropower generation) and tributary contributions. Stage differences also occur between image years due to natural hydrologic variability. To control for spatial-temporal differences in stage between and within classified images, a normalization and thresholding procedure was used to design the response variable (m_i):

$$m_i = \begin{cases} 1, & 1 > \frac{A_{es_{ijk}}}{\langle A_{es} \rangle_{jk}} \\ 0, & 1 < \frac{A_{es_{ijk}}}{\langle A_{es} \rangle_{jk}}, \end{cases} \tag{6}$$

where $A_{es_{ijk}}$ is the summed total of continuous emergent sand within polygon i greater than 0.2 ha, within steady-flow reach j, in image year k, and $\langle A_{es} \rangle_{jk}$ is mean area of emergent sand for extraction polygons within steady-flow segment j (black horizontal lines in Figure 3b). The minimum number of steady-flow segments j in each image year k was 3 because confluences of major tributaries (Elkhorn River and Salt Creek) are known flow-change boundaries. Additional steady-flow reach boundaries j were defined at abrupt shifts in the moving average of emergent sand area for each image year k (red line in Figure 3b). The supporting information contains additional method details.

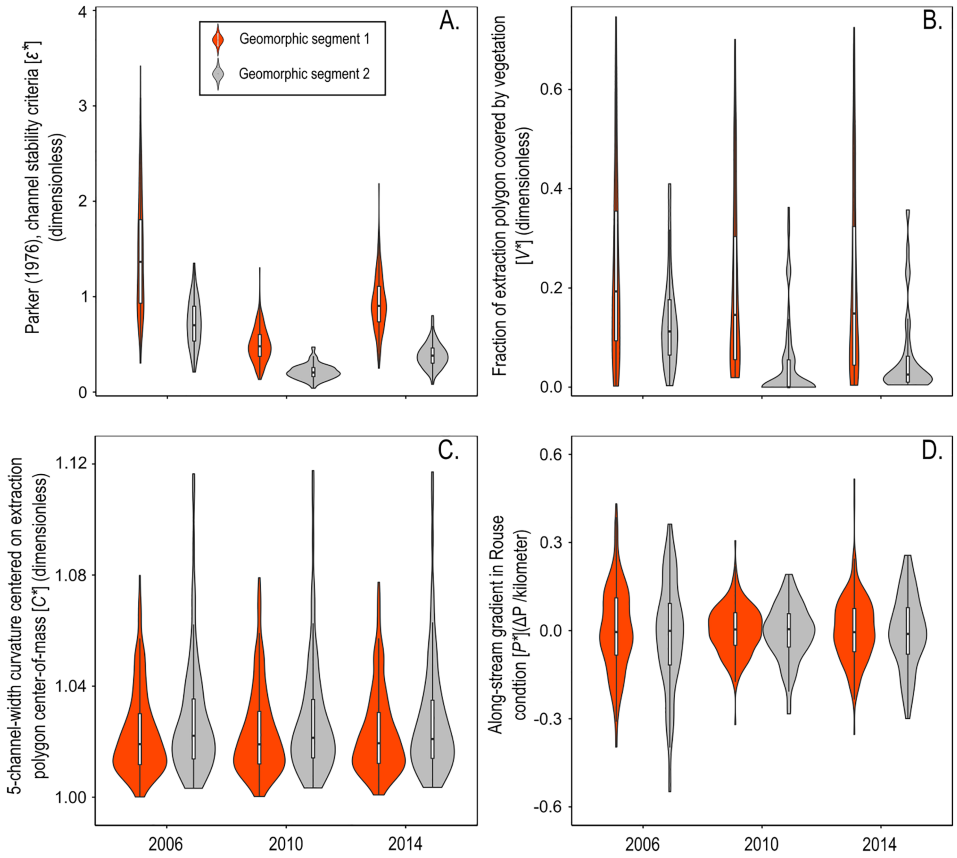

Figure 4. Violin plots showing distributions of channel characteristics calculated within 500-m-long extraction polygons along the lower Platte River in eastern Nebraska for three different years. Box-and-whisker boundaries within violin plots represent the interquartile range of the data, and horizontal line within the box is the median. Geomorphic segments are differentiated by a distinct change in channel slope at their boundary. Geomorphic Segment 1 is from 52 to 163 km, and Geomorphic Segment 2 is from 6.5 to 52 km upstream from the Missouri River.

The threshold of 0.2 ha was chosen because it was the mean emergent area of the four smallest sandbars with nests measured during our field surveys [0.06, 0.23, 0.26, and 0.27 ha]. This threshold value, although small, is roughly double the habitat quality threshold used in the Platte River Recovery Program on the central Platte River (Platte River Recovery Program, 2015). We consider this larger threshold reasonable because it is consistent with field observations, and the larger channel and peak discharges of the LPR would be expected to cause average sandbar size to be larger than in the central Platte River.

2.1.2. Model

Logistic regression is used to quantify the relative contribution of explanatory variables $(\varepsilon^*, V^*, C^*, P^*)$ on m_i. Since m_i is binary, our data model assumes it is Bernoulli distributed with probability of exceedance denoted by θ_i, and logit of θ_i is modeled as a linear function of the four predictor variables. Notationally, the data model is as follows:

$$m_i|\theta_i \sim Bern(\theta_i) \tag{7}$$

$$logit(\theta_i) = \alpha_o + \alpha_1\varepsilon_i^* + \alpha_2 V_i^* + \alpha_3 C_i^* + \alpha_4 P_i^*, \tag{8}$$

where $logit(\theta_i)$ is the *logit* link function $log\left(\frac{\theta_i}{1-\theta_i}\right)$ and α_j are model coefficients. To minimize the impact of priors on parameter estimates, diffuse priors were assumed for model parameters (i.e., $\alpha_j \sim N[\mu_j = 0, \frac{1}{\sigma} = 0.0001]$). The logistic model was implemented using a Bayesian framework in language *R* (R Core Team, 2017; Version 3.4.3) and the Gibbs sampling package "Rjags" (Plummer et al., 2016).

The Bayesian analysis assumed data from individual years was independent of other years and used 1,000 burn-in steps with three Markov chains of 20,000 steps each to update prior distributions and generate

posterior predictive distributions for α_j and θ. The model was used to generate posterior distributions of θ for polygons with tern and plover nests in each image year. Nesting location data were provided by the Nebraska Game and Parks Commission.

2.2. Methods Part 2: Emergent Sandbar Top-Surface Flow-Response Dynamics

The term "sandbar height" refers to a sandbar top-surface elevation measurement relative to a water surface datum:

$$Z_{\hat{B}_{k_j}} = Z_{B_{k_j}} - Z_{W_{k_j}}, \tag{9}$$

where $Z_{\hat{B}_{k_j}}$ is the elevation of sandbar top-surface elevation measurement $Z_{B_{k_j}}$, made in reach k, relative to a nearby water surface elevation $Z_{W_{k_j}}$. If the measurements of $Z_{B_{k_j}}$ and $Z_{W_{k_j}}$ are precise ($< \pm 0.01$ m), and $Z_{\hat{B}_{k_j}}$ is large (>0.10 m) the relative measurement error is small (Taylor, 1996). The larger source of error occurs when attempting to compare $Z_{\hat{B}_{k_j}}$ to another measurement made at a different time or location within the same river reach ($j = 1$ vs. $j = 2$) or a different river reach ($k = 1$ vs. $k = 2$) because $Z_{W_{k_j}}$ changes with river discharge, which is variable over time and space. Alexander et al. (2013) accounted for this error using a time-of-travel calculation to estimate local discharge ($\hat{Q}_{k_j}$) at the time $Z_{\hat{B}_{k_j}}$ is made. They used a U.S. Geological Survey (USGS) rating table to reference measurements of $Z_{B_{k_j}}$ to a common water surface elevation datum, in that case, the stage of the mean annual discharge:

$$Z_{\tilde{\hat{B}}_{k_j}} = Z_{B_{k_j}} - Z_{W_{k_j}} - Z_{\hat{Q}_{k_j}} - Z_{\bar{Q}_k}, \tag{10}$$

where $Z_{\hat{Q}_{k_j}}$ is the stage of $\hat{Q}_{k_j}$ at a streamgage representing hydraulic conditions in reach k and $Z_{\bar{Q}_k}$ is the stage of the mean annual discharge ($\bar{Q}_k$) in reach k at the same streamgage. The right two terms in equation (8) are stages in meters above the arbitrary datum of the streamgage and are obtained via lookup on a streamgage rating table using discharge values for $\hat{Q}_{k_j}$ and $\bar{Q}_k$ as inputs.

Here, a two-level hierarchical regression model was used to generate models of growth rates of sandbar top-surface heights relative to formative flood stages. The first level used discharge-stage rating relations to reference field measurements of sandbar heights and formative flood stages to a common datum. The rating relations took the log linear form common to many rivers (Kennedy, 1984). The second level used heights generated in the first level to model growth rates of sandbar top-surface height and formative flood stage relative to formative flood magnitude. Simple linear models were sufficient to describe growth rates because they occurred at discharges beyond the inflection point of the log linear rating relations in Level 1.

2.2.1. Hierarchical Model Level 1: Data and Models

The sandbar top-surface elevation measurements used herein were made over 4 years and along 160 km of river. Level 1 of our hierarchical model accounted for spatial variation in river stage for a given discharge using the erogodic assumption that temporal variation of observed stage for a discharge measured at a representative streamgage approximates the spatial variation in stage for that discharge. Restated, the residuals of the regression model built using measurements of river discharge and stage taken over many years at a single location (a streamgage), approximate the spatial variation in river stage for discharges within the river segment represented by the gage.

Paired field observations of river stage and discharge from USGS Streamflow Gaging Stations 06796000 and 06801000 were used to generate linear regression models (rating relations) between river discharge and stage for GS1 and GS2, respectively. Although the study area can be subdivided into five hydrologic segments, represented by five different streamgages, only data from these two streamgages were used to generate the Level 1 rating relations because a preliminary analysis indicated the main influences on model parameters were river slope and period of record. Data from Streamgages 0679600 and 06801000 were chosen because they have the longest periods of record within their respective geomorphic segments (GS1 and GS2) and thus incorporate more sample pairs and represent a larger range of flow conditions. To avoid issues with datum changes and ice-influenced stages, observations from previous station locations and those taken during winter months (November–March) were excluded.

The data model for the rating relations in GS1 and GS2 follows the general form of a log linear regression (Kennedy, 1984):

$$log_{10}(Z_{k_i})|\mu_i, \sigma \sim N(\mu_i, \sigma) \tag{11}$$

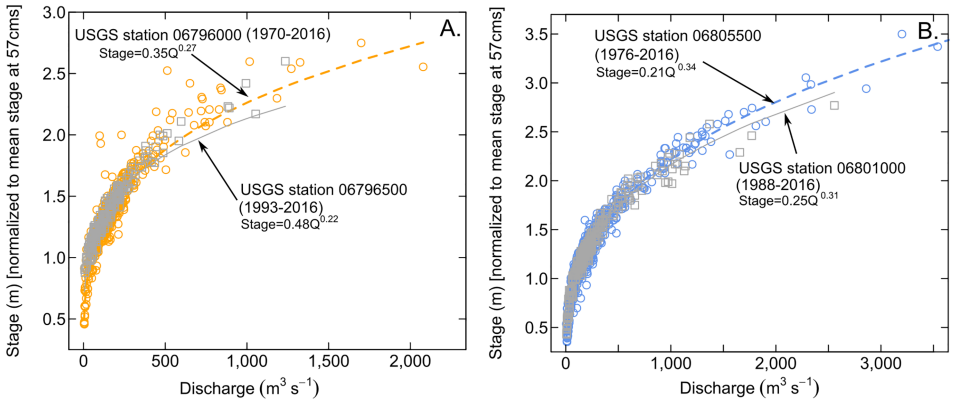

Figure 5. Scatterplots showing power law linear regression relationships between measurements of river discharge and river stage at U.S. Geological Survey streamflow gaging stations representing two different geomorphic segments of the lower Platte River, Eastern Nebraska. (a) Geomorphic Segment 1; (2) Geomorphic Segment 2. Circles and dashed lines indicate regression relationship for streamgage with longer period of record; squares and solid lines indicate relation for streamgage with shorter period of record. Only the relationships for the longer period-of-record streamgages were used to estimate reference stages for sandbar height indexing and spatially averaged stage of formative flood discharge.

$$\mu_i = \beta_{k_0} + \beta_{k_1} * log_{10}(Q_{k_i}), \tag{12}$$

where Z_{k_i} is an observation of stage in meters at a streamgage representing hydraulic conditions in geomorphic segment k, Q_{k_i} is an observation of river discharge in cubic meters per second, and β_{0_k} and β_{1_k} are model parameters. Bayesian linear regression was used to generate posterior estimates for β_{0_k} and β_{1_k}. As before, the Bayesian regression was implemented in language *R* (R Core Team, 2017; Version 3.4.3) using the Gibbs sampling package "Rjags" (Plummer et al., 2016). The regression assumed diffuse priors for model parameters (i.e., $\beta_{j_k} \sim N[\mu_{j_k} = 0, \frac{1}{\sigma} = 0.0001]$) and a wide prior variance on Z_{k_i} ($\sigma^2 \sim \Gamma^{-1}[0.01, 0.01]$, where Γ^{-1} is the inverse gamma distribution). Posterior estimates of model parameters are shown as the equations for the dashed regression lines in Figure 5.

2.2.2. Hierarchical Model Level 2: Data

Emergent sandbars in the LPR generally have a flat, table-like top surface, which slopes in the downstream direction at approximately the same grade as the water surface (Smith, 1971; Figure 2). The sparse-grid survey method of Alexander et al. (2013) was used to take field measurements of emergent sandbar top-surface elevations from four different years (Table 2). These data were used to characterize relations between formative flood magnitude (spring instantaneous peak prior to measurement) and sandbar top-surface elevation. With the exception of the survey in April 2011, which targeted emergent sandbars formed during the ~20-year flood of July 2010, the remaining field surveys occurred during baseflow conditions after spring flood recession.

Emergent sandbars were selected for surveying in one of two ways: (1) the two surveys done in 2011 (described in Alexander et al., 2013), focused only on GS2, and selected all emergent sandbars larger than 0.8 ha; and (2) the surveys of 2013 and 2014 selected the largest emergent sandbar visible once per kilometer. The surveys taken in 2011 used a laser level to measure local sandbar top-surface and water surface elevations and a differential global positioning system to record the horizontal locations of the measurements. The surveys of 2013 and 2014 covered the entire field area and used real-time kinematic GPS rovers connected to a virtual reference station network.

Sandbar height measurements ($Z_{B_{k_j}}$) were taken along an evenly spaced grid and had a reference water surface elevation measurement ($Z_{W_{k_j}}$) taken at the edge of the sandbar (Figure 6). The time-of-travel calculation presented by Alexander et al. (2013) was used to generate estimates of local river discharge for each reference water surface elevation ($\hat{Q}_{k_{ij}}$). Using inputs of the mean annual discharge in each hydrologic segment ($\bar{Q}_k$), peak flood (formative flood) magnitude ($\bar{\bar{Q}}_{k_i}$) for each observation year, and $\hat{Q}_{k_{ij}}$, the rating relations in Level 1 were used to generate posterior predictions of the spatially averaged stages of the mean annual flow for each hydrologic reach ($\langle Z \rangle_{\bar{Q}_k}$), the spatially averaged stages of the formative flood ($\langle Z \rangle_{\bar{\bar{Q}}_{k_i}}$), and discharges at the time of reference water surface elevations ($\langle Z \rangle_{\hat{Q}_{k_{ij}}}$). Posterior estimates of $\langle Z \rangle_{\bar{Q}_k}$ were subtracted from

Table 2
Summary of Sandbar Height Field Measurements in Lower Platte River Study Area

		Survey period			
	Hydrologic Segment[b]	April 2011	July 2011	July 2013	July 2014
1. [RKM 97.1 to 163.2; USGS-06796000]					
Geomorphic Segment 1[a]	no. bars surveyed	—	—	54	69
	no. height measurements	—	—	333	394
	no. replicate measurements[c]	—	—	18	30
2. [RKM 69.7 to 97.1; USGS-06796500]					
	no. bars surveyed	—	—	19	34
	no. height measurements	—	—	104	211
	no. replicate measurements[a]	—	—	12	14
3. [RKM 52.2 to 69.7; USGS-06796550]					
	no. bars surveyed	—	—	9	16
	no. height measurements	—	—	20	98
	no. replicate measurements[a]	—	—	0	7
4. [RKM 41 to 52.2; USGS - 06801000]					
Geomorphic Segment 2[a]	no. bars surveyed	—	—	9	17
	no. height measurements	—	—	64	122
	no. replicate measurements	—	—	7	5
5. [RKM 6 to 41; USGS-06805500]					
	no. bars surveyed	25	38	22	33
	no. height measurements	195	283	126	233
	no. replicate measurements[a]	30	28	20	5

[a] Geomorphic reaches are defined by a decrease in river slope downstream from Elkhorn River. [b] Boundaries of hydrologic segments are shown by river kilometer (RKM) and associated representative U.S. Geological Survey (USGS) stream gage number. [c]Replicate measurements were taken for quality control

posterior estimates of $\langle Z \rangle_{\bar{Q}_{k_i}}$ within the Level 1 model to create posterior estimates of indexed spatially averaged formative flood stage ($\langle Z \rangle_{\underline{\bar{Q}}_{k_i}}$). Posterior estimates of $\langle Z \rangle_{\hat{Q}_{k_{ij}}}$ and $\langle Z \rangle_{\bar{Q}_k}$ replaced the last two terms in equation (8), respectively, to generate posterior estimates of indexed sandbar height measurements ($Z_{\underline{\hat{B}}_{k_{ij}}}$).

Herein we use the term "genetic sandbar" for sandbars with field evidence associating them with the most recent peak flood and "remnant sandbar" for those sandbars formed by some prior flood. Evidence of a genetic sandbar included: (1) barren or sparse vegetation indicating the sandbar top was less than several weeks old; (2) dry top surface with presence of sand ripples indicating sandbar top surface emerged from recent high-flow event; (3) absence of ice scour and plowing features indicating sandbar was not present during winter months [this evidence was ignored for the April 2011 survey]; (4) absence of o-horizon within stratigraphy exposed sandbar banks indicating recent deposition over a lower, vegetated surface.

2.2.3. Hierarchical Model Level 2: Model

Bayesian regression models were used to characterize flow-response dynamics of sandbar top-surface heights and formative flood stage relative to formative flood magnitude. The data model for the sandbar top-surface-heights relative to formative flood magnitude took a simple, linear form:

$$Z_{\underline{\hat{B}}_{k_{ij}}} | \mu_i, \sigma \sim N(\mu_i, \sigma) \tag{13}$$

$$\mu_i = \gamma_{k_0} + \gamma_{k_1}(Q_{k_i}), \tag{14}$$

where $Z_{\underline{\hat{B}}_{k_{ij}}}$ is an indexed sandbar height measurement in units of meters, Q_{k_i} is the formative flood magnitude in units of cubic meters per second, γ_{k_o} is the model intercept and γ_{k_1} is the model slope. The data model used to characterize the flow-response dynamics of the formative flood stage was as follows:

$$\langle Z \rangle_{\underline{\bar{Q}}_{k_i}} | \mu_i, \sigma \sim N(\mu_i, \sigma) \tag{15}$$

Table 3
Summary of Seasonal Survey Periods in Lower Platte River

Survey	Start date	End date	Mean discharge (m^3/s)[b]	Mean stage (meters)[c]
1	4-6-2011	4-12-2011	319	1.35#
2	7-26-2011	8-2-2011	305	1.32 #
3	10-31-2011	11-3-2011	242	1.19 #
4	4-27-2012	5-3-2012	228	1.16 #

[a]Flow data from U.S. Geological Survey Station No. 06805500, the Platte River at Louisville, Nebraska. [a]Stage data from rating table for U.S. Geological Survey Station No. 06805500, the Platte River at Louisville, Nebraska. Rating table acquired from National Water Information System on 1 March 2015.

$$\mu_i = \delta_{k_0} + \delta_{k_1}(Q_{k_i}), \tag{16}$$

where $\langle Z \rangle_{\underline{\bar{Q}}_{k_i}}$ is the indexed spatially averaged stage of a formative flood in units of meters, δ_{k_o} is the model intercept, and δ_{k_1} is the model slope. Both Bayesian regressions were implemented in language *R* (R Core Team, 2017; Version 3.4.3) using the Gibbs sampling package "Rjags" (Plummer et al., 2016). As before, the regressions assumed diffuse priors for model parameters and a wide prior variance on $Z_{\underline{\hat{B}}_{k_{ij}}}$ and $\langle Z \rangle_{\underline{\bar{Q}}_{k_i}}$.

Lastly, differences in sandbar height distributions were examined for two scenarios: (1) height of large barren sandbars before and after the 2011 spring flood and (2) depositional heights of genetic sandbars relative to vegetated remnant sandbars. Posterior predictions of top-surface heights from the Level 2 hierarchical model ($Z_{\underline{\hat{B}}_{k_{ij}}}$) are used to model group means as follows:

$$\langle Z_{\bar{Q}_k} \rangle_j | \mu_j \sim N(\mu_j, \sigma), \tag{17}$$

where *j* represents a group. Bayesian statistical analysis was used to generate posterior probabilities of the difference between group means being greater than 0:

$$P[(\langle Z_{\bar{Q}_k} \rangle_1 - \langle Z_{\bar{Q}_k} \rangle_2) > 0 | \mu_1, \mu_2] \tag{18}$$

where "1" and "2" represent a sandbar group (i.e., barren, remnant, or vegetated top surface). As before, diffuse priors were used to initiate the analysis.

2.3. Methods Part 3: Emergent Sandbar Erosion Dynamics

Field surveys of emergent sandbar areas were used to quantify postdeposition flow-response dynamics from one nesting season to the next (a full year). Three measures were used to quantify dynamics: (1) change

Table 4
Posterior Summary Statistics of Logistic Regression Model Coefficients for Variables Used to Predict Potential for Presence/Absence of Emergent Sandbar Area Exceeding a Reach-Scale Mean

Coefficient (variable)	μ	σ	2.5%	97.5%
α_0 (intercept)	−0.27	0.07	−0.40	−0.14
α_1 (ε^*)	0.18	0.07	0.04	0.32
α_2 (V^*)	−0.14	0.07	−0.27	0.00
α_3 (C^*)	0.00	0.07	−0.14	0.13
α_4 (P^*)	0.25	0.07	0.11	0.39

Note. All values shown are for standardized coefficients; μ, mean; σ, standard deviation; 2.5%, 97.5% are the bound of the central 95% of values in the posterior distribution.

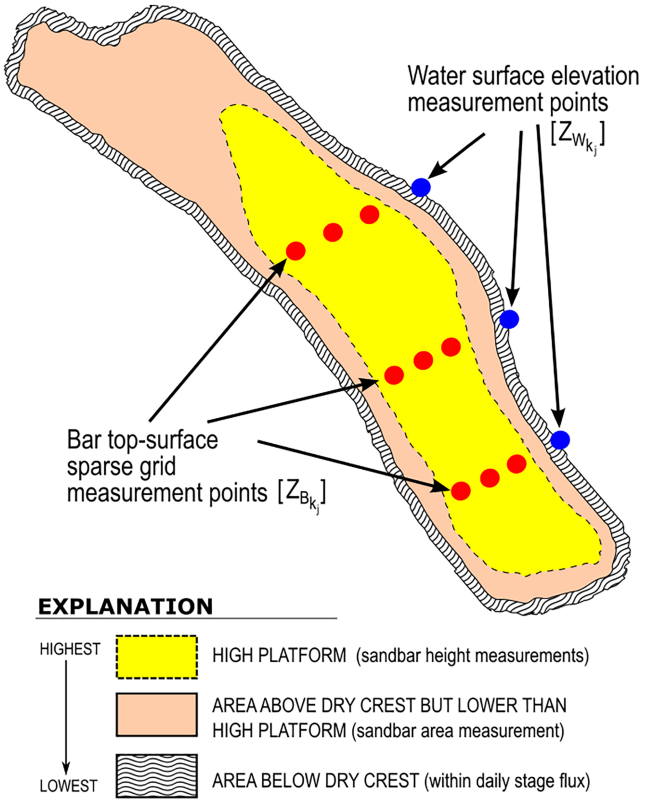

Figure 6. Schematic diagram showing typical layout of sparse-grid survey measurements of emergent sandbar top surfaces. Adapted from Alexander et al. (2013).

in emergent planimetric area of a sandbar; (2) persistence, defined as the temporal change in number of sandbars with time; and (3) deformation, defined as change in shape of sandbars with time.

2.3.1. Data

Four-sequential ground surveys in GS2 were used to track two sets of emergent sandbars between April 2011 and May 2012 (Table 3). The sandbars could not be tracked beyond May of 2012 because extreme drought conditions in the summer of 2012 made boat transport impossible and many sandbars became densely vegetated that year. Nonetheless, sandbar erosion rates from the across-season surveys compare favorably with erosion rates obtained from a within-season survey done in 2014 (see supporting information).

For each survey, the planimetric area of all sandbars larger than 0.8 ha was measured by walking the margin of the sandbar above the daily hydrocycle crest (Figure 5) and automatically logging position every 3 m using a hand-held differential global positioning system. These points were linked to create a polygon of each sandbar. Only sandbars larger than 0.8 ha were surveyed because local bird ecologists indicated sandbars smaller than this were rarely used as nesting habitat. We later measured sandbars that were smaller (see "Methods Part 1"). Regardless, very small sandbars are more difficult to accurately identify as "the same" and track between surveys. The four surveys were conducted during low-magnitude discharges and, because stages during subsequent surveys were lower or equivalent to the first survey, measured changes in planimetric area were conservative (Table 2).

Two sets of emergent sandbars were tracked to quantify sandbar persistence. The first set comprised remnants of genetic sandbars created by the spring flood of 2010 (3,851 $m^3\ s^{-1}$, R.I. $\approx$ 20 years; $n = 25$). The second set comprised genetic sandbars present in the second survey, but not in the first (i.e., formed during the spring 2011 flood; 1,286 $m^3\ s^{-1}$, R.I. $\approx$ 2 years; $n = 19$). Surveyed sandbars consisted of midchannel and bank-attached (attached to a vegetated island or floodplain), and ranged in length from from 72 to 1,070 m, and 0.26 to 16.2 ha in emergent area.

2.3.2. Quantitative Measures and Modeling

Planimetric sandbar erosion rate between observations was quantified as follows:

$$\frac{dA}{dt} = E_{i-j} = \frac{A_i - A_j}{d_j - d_i}, \tag{19}$$

where E_{i_j} is planimetric erosion rate in square meters per day between observations i and j, A is planimetric area measured above the daily high water mark, and d is day, measured as day of year. The equation is set up such that an increase in sandbar area would result in a negative erosion rate. Erosion was calculated using two methods: (1) changes in net planimetric area and (2) changes in gross area relative to the original survey. The first method was simply the difference in total emergent sandbar area between two successive surveys. The second method used successive polygon intersections between time steps (i.e., 1–2, 2–3, and 3–4), while keeping only the area common between intersections (Figure 7). We call this second, more conservative measure "gross erosion" because it tracks erosion of original sandbar mass, and does not allow for area to increase.

Emergent sandbar persistence was tracked as an attrition rate:

$$L_{o-i} = \frac{n_o - n_i}{n_o} * 100, \tag{20}$$

where L is the attrition rate between observations from the original set o and some later observation i, n_o is number of sandbars observed in the original set, and n_i is the number of sandbars remaining from the original set during observation i.

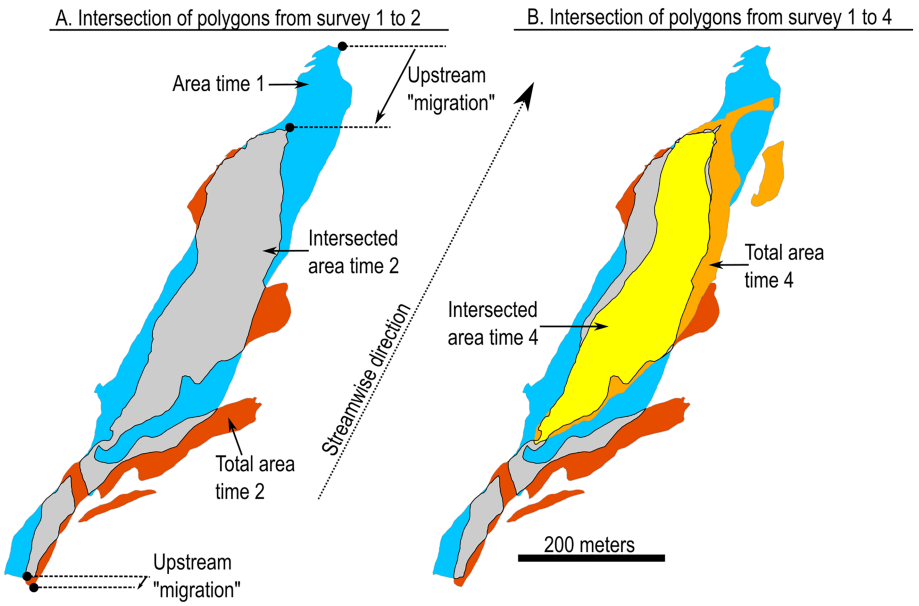

Figure 7. Schematics of emergent sandbar polygons illustrating examples of methods to quantify planimetric rates of sandbar erosion. (a) Example of polygons from two successive surveys; net erosion is the difference in total emergent sand areas between the two surveys; gross erosion is the exposed area of sand common between surveys (gray area). (B) Gross erosion after four successive surveys by intersection of only the common area of polygons from successive surveys. The yellow polygon is the area of emergent sand from the first survey remaining during the fourth survey. Migration of sandbar ends between surveys is tracked using the most-upstream and most-downstream points in the respective polygons. The method is only conservative if discharge during successive surveys is the same or lower than the first survey.

Sandbar deformation was quantified using two measures: (1) translation and (2) width. Sandbar translation was tracked by quantifying changes in the centerline location of the upstream and downstream-most points on each sandbar (Figure 7). Translation distances were quantified for the high-flow period between Surveys 1 and 2 and over the low-flow period between Surveys 2 and 4. Translation distances were normalized by dividing by the original sandbar length:

$$\Delta S_{x_{i-j}} = \frac{S_{x_i} - S_{x_j}}{S_{u_o} - S_{d_o}} \tag{21}$$

where $\Delta S_{x_{i-j}}$ is the change in channel centerline location S of boundary x (upstream or downstream), between observations i and j relative to the original along-stream length of the sandbar $S_{u_o} - S_{d_o}$, with u and d specifying the upstream and downstream boundary locations, respectively. Translation distances were tracked relative to net and gross emergent sandbar area. Mean emergent sandbar width relative to mean channel width was calculated for all four surveys as follows:

$$\bar{W}_i = \frac{\left(\frac{A_i}{S_{u_i} - S_{h_i}}\right)}{\langle W_{ch} \rangle}, \tag{22}$$

where $\bar{W}$ is the mean sandbar width at observation i and $\langle W_{ch} \rangle$ is the spatially averaged active-channel width in GS2 (500 m).

Lastly, following the work of Buenau et al. (2014), the decay rate of sandbar area in the LPR (λ) was estimated using linear regression with a term for exponential decay as a function of time. The data model was as follows:

$$log(A_{tot_i}) | \mu_i, \sigma \sim N(\mu_i, \sigma^2) \tag{23}$$

$$\mu_i = log(A_o) + \lambda t, \tag{24}$$

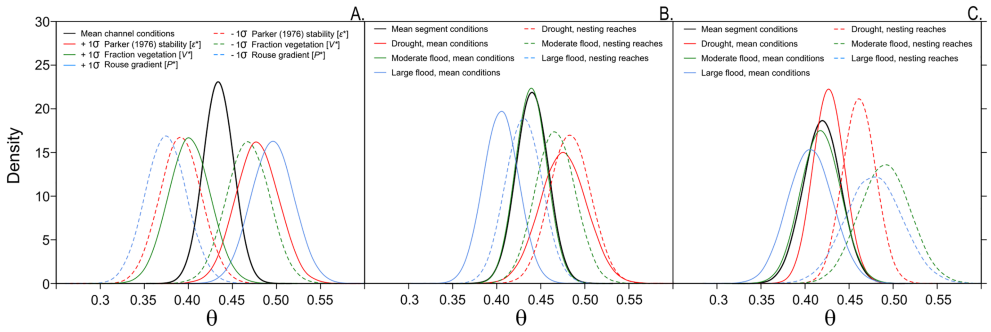

Figure 8. Bayesian posterior distributions of probability (θ) of a river reach having continuous emergent-sand-area exceeding a segment-scale mean for the lower Platte River in eastern Nebraska: (a) Posterior distributions of θ for mean channel conditions and single-standard deviation in each regression variables [σ = standard deviation]; (b) posterior distributions for mean channel and varying hydrologic conditions in Geomorphic Segment 1. (c) Same as (b) but for Geomorphic Segment 2. Geomorphic segments are differentiated by a distinct change in channel slope at their boundary. Geomorphic Segment 1 is from 52 to 163 km, and Geomorphic Segment 2 is from 6.5 to 52 km upstream from the Missouri River confluence.

where A_{tot_i} is the total remaining area of a set of emergent sandbars as function of time t, in days, and A_o is the original measured total emergent area of a sandbar sample set i, and λ is the unknown decay constant. Model parameters were estimated using a Bayesian statistical analysis, which, as before, assumed diffuse priors (i.e., $\mu = 0$ and $\sigma^2 \sim \Gamma^{-1}[0.01, 0.01]$).

3. Results

3.1. Results Part 1: Emergent Sandbar Deposition Potential

Bayesian posterior distributions of the partial slope coefficients from the logistic regression for stability criterion (ε^*) and gradient in Rouse conditions (P^*) are positive and exclude 0 (Table 4), indicating they contribute to increases in potential for a reach to have emergent sandbar area greater than the segment mean (θ). The 95% posterior credible intervals for the coefficients associated with fraction of polygon covered by vegetation (V^*) and channel curvature (C^*) contain zero. However, the credible interval for C^* is nearly centered on zero (−0.13, 0.14), indicating no influence on θ, while the interval for V^* indicates a 97.4% chance the coefficient is negative (Table 4). The lack of influence C^* is not surprising given the weakly meandering nature of the LPR.

Of the extraction polygons that had documented nesting by interior least terns and/or piping plover, 80% had m_i values of 1, suggesting the response variable was a good indicator of ESH quality. Posterior distributions of θ for spatial-temporal mean (system-wide) channel conditions had a mean of 0.43 (credible interval = [0.40, 0.47]), indicating the probability of any random reach having continuous emergent sand area exceeding the segment mean is about 7% less than a coin toss. Simulated increases of one standard deviation from the system-wide mean values for P^* and ε^* caused the mean value of θ to increase by more than 10% to 0.50 [0.45, 0.54] and 0.48 [0.43, 0.53], respectively, whereas a single standard deviation increase in V^* causes θ to decrease to 0.40 [0.36, 0.45].

Posterior distributions of θ were also generated for mean conditions in each geomorphic segment, for ambient conditions in each segment after small (2006), moderate (2014), and large (2010) floods and for reaches with observed nests (Figures 8b and 8c). Values of θ for temporally averaged conditions are slightly higher in GS1 ($\theta = 0.44$ [0.41, 0.47]) than GS2 ($\theta = 0.42$ [0.38, 0.46]). Values of θ following a small flood increase in GS1 (θ=0.48 [0.43, 0.53]) and GS2 ($\theta = 0.43$ [0.39, 0.46]), whereas θ values after a large flood decrease to 0.41 in both segments. Values of θ after a moderate flood were nearly identical to temporally averaged values.

Posterior estimates of θ for ambient conditions in reaches with bird nests were always larger than estimates for ambient conditions in geomorphic segments (Figures 8b and 8c). For one case, small flood conditions in GS1, θ values for ambient conditions were nearly identical to those with nests. Differences in θ between reaches with nests and ambient conditions tended to increase with increasing discharge and were larger in GS2 than GS1. For conditions following moderate and large floods in GS2, θ values in reaches with bird nests

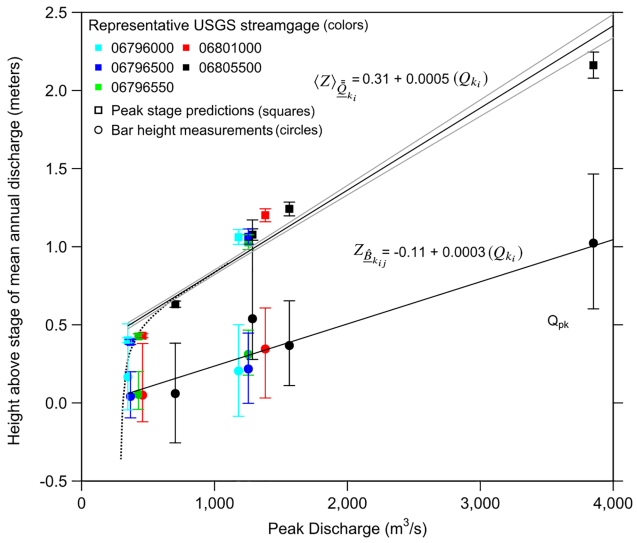

Figure 9. Relationships between river discharge, stage of peak flow, and sandbar top-surface height in the lower Platte River, eastern Nebraska. Error bars on height of peak stage are the Bayesian 95% posterior credible intervals. Error bars on sandbar top heights show the inner 95% Bayesian posterior predictions of sandbar top height measurements for each survey in each hydrologic reach. The dotted line shows the estimated model of the discharge-peak-stage relation if a log linear model were used.

were more than 15% larger than segment ambient conditions; in GS1, reaches with nests were just over 6% larger than ambient conditions.

3.2. Results Part 2: Emergent Sandbar Top-Surface Flow-Response Dynamics

Relations between formative flood magnitude, reference sandbar top-surface height ($Z_{\hat{\underline{B}}_{k_{ij}}}$), and formative flood stage ($\langle Z \rangle_{\bar{\underline{Q}}_{k_i}}$) suggest that, beyond discharges of about 200 $m^3\ s^{-1}$ both quantities increase linearly but the rate of increase in $Z_{\hat{\underline{B}}_{k_{ij}}}$ lags that of $\langle Z \rangle_{\bar{\underline{Q}}_{k_i}}$. The slope of the line describing growth in $Z_{\hat{\underline{B}}_{k_{ij}}}$ (γ_{k_1}) is approximately 3 cm per 100 $m^3\ s^{-1}$ (cm/100 $m^3\ s^{-1}$), while the rate of growth in $\langle Z \rangle_{\bar{\underline{Q}}_{k_i}}$ (δ_{k_1}) is approximately 5 cm/100 $m^3\ s^{-1}$. We term the difference in height between sandbar top-surface and formative flood stage, the "depositional gap."

The divergence between γ_{k_1} and δ_{k_1} of about 2 cm per 100 $m^3\ s^{-1}$, while small, is not trivial. Posterior distributions of γ_{k_1} and δ_{k_1} do not overlap, and the process is supported by anecdotes and observations that, while limited, indicate that water depth over sandbar tops increases in scale from centimeters during low-magnitude discharges (Brice, 1964; Dilbone et al., 2018; Mohrig, 1994; Smith, 1971) to meters during floods (Ashworth et al., 2000; Crowley, 1983). The regression relation between $Z_{\hat{\underline{B}}_{k_{ij}}}$ and discharge has a slightly negative intercept, which is expected because top-surfaces cannot grow higher than their formative stage.

The growth process of the mean depositional gap is well approximated by the divergence of the lines shown in Figure 9, but there is greater uncertainty for prediction of random bar top-surface heights. Error bars on the measured sandbar top-surface heights shown in Figure 9 depict the inner 95% of measured sandbar heights and show that the credible range of bar top heights span as much as 1 m about the mean. Additionally, our data set only captured sandbar heights for one very high magnitude discharge in GS1. However, removal of those data only increase γ_{k_1} by 1 mm (3.1 cm/100 $m^3\ s^{-1}$), indicating weak leverage on model parameter estimates.

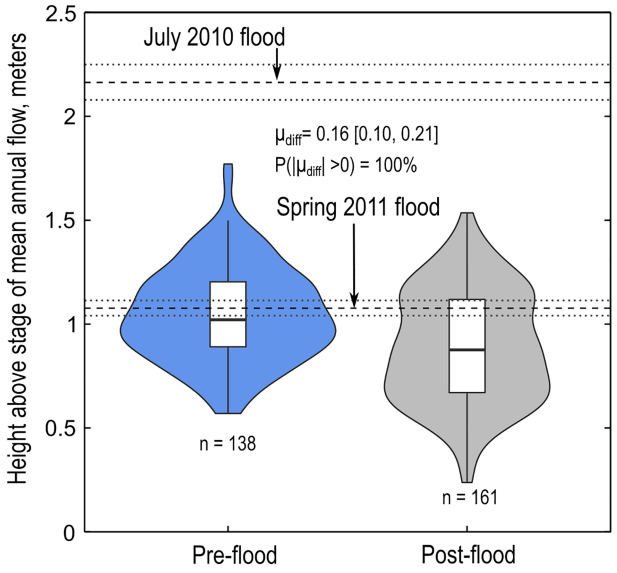

Figure 10. Violin plots showing distributions of sandbar top-surface-height measurements taken on 12 sandbars before and after the spring flood of 2011, a flood of approximately 2-year return interval. The sandbars were originally created by a flood of 20-year return interval and were only sparsely vegetated, likely because of their very high top surface. Black lines indicate mean predicted stage for each flood; gray lines indicate Bayesian 95% posterior credible intervals for the mean stage.

Tracking of changes in sandbar top-surface height after floods indicates that barren sandbars were lowered by subsequent flooding, even if the flood stage was lower than the original sandbar top-surface (Figure 10). Twelve barren sandbars originally formed by the large flood of July 2010 (~20-year R.I.) were measured before and after the 2011 flood (~2-year R.I.). Posterior estimates of population means indicate the 2011 flood lowered remnant top surfaces by about 16 cm [0.10 to 0.21]. The fact that the stage of the flood of 2011 was not capable of completely inundating all sandbar top-surfaces formed by the 2010 flood suggests that lateral erosion (emergent sandbar bank calving) was the primary erosion mechanism.

Alternatively, differences in measured height of genetic and vegetated sandbars in 2013 and 2014 indicate that vegetated sandbars vertically accreted higher than genetic sandbars. The vegetated remnant sandbars likely formed in 2012 and 2013 when low-magnitude peak flows and prolonged summer low flows promoted vegetation establishment. Posterior estimates of population means indicated a difference of −0.05 m (−0.02,−0.09) between genetic and vegetated sandbars in 2013 and −0.07 m (−0.05,−0.10) in 2014 (Figure 11). Field observations indicated that this deposition generally did not cause vegetation mortality.

3.3. Results Part 3: Emergent Sandbar Erosion Dynamics

The terms "gross" and "net" are used here in reference to erosion measured by tracking (1) changes in the original sandbar area and (2) changes

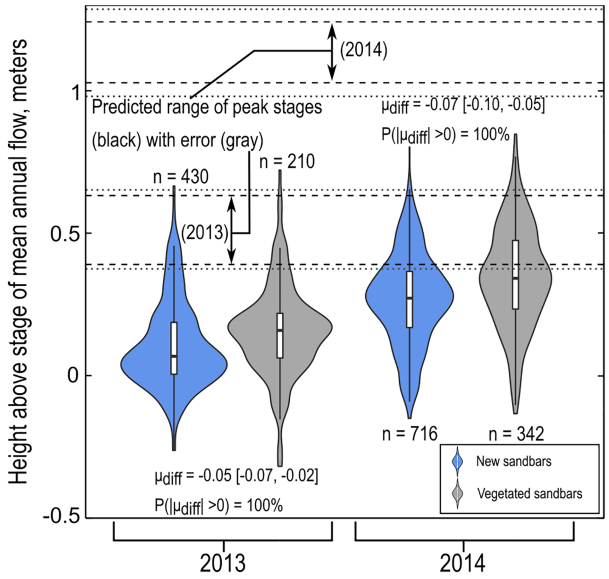

Figure 11. Box-and-whisker plots showing distributions of sandbar top-surface-height measurements for new bars (bars created by most recent spring flood) and bars that had vegetation predating the spring-flood event of the year shown.

in total measured sandbar area, respectively. Table 5 summarizes these values by sandbar type and the erosion dynamics of two sets of sandbars tracked across four seasons from April 2011 to April 2012. The high-flow period was April to July 2011, and low-flow periods were July 2011 to November 2011 (fall low flow) and November 2011 to April 2012 (winter low flow).

Set 1 was tracked across all four seasons and had total attrition rates of 69% and 25% for midchannel and bank-attached sandbars, respectively. Most of the losses in Set 1 occurred during the high-flow period, when nearly half of midchannel sandbars were completely eroded. Set 2 sandbars formed during the high-flow period and were tracked starting in July 2011. The losses in both number and area of emergent sandbars from Set 1 during the spring peak of 2011 were partially offset by gains from Set 2. No bank-attached sandbars were lost from Set 2 over the tracking period, whereas midchannel sandbars from this set had a 71% attrition rate, mostly over the winter low-flow period.

Gross erosion rate, the most conservative measure of erosion between periods, was highest during the high-flow period in the spring of 2011 at around 10^{-1} ha/day and was consistently of order 10^{-2} ha/day during the low-flow periods. The value of using gross erosion is evident in the effect of the 0.13-m stage decrease between the July and November 2011 surveys (Table 3), which resulted in a large negative net erosion rate (indicating deposition), yet gross erosion rate remained at a positive, low-magnitude value, similar to the successive low-flow period. Despite a slightly lower stage in April 2012, both net and gross sandbar area decreased between July 2011 and April 2012, indicating some of the emergent sandbar area exposed between July and November 2011 was eroded during the winter months. Erosion rates from July 2011 to April 2012 are of the same magnitude as those measured during the nesting season in 2014 (see the supporting information).

The effect of discharge on sandbar persistence is manifest when comparing sandbars of different starting size and attachment conditions (Table 5). Persistent sandbars started larger than the mean starting size of their sample set, whereas eroded sandbars started smaller than set means. Importantly, mean starting size of persistent sandbars was 2 to 3 times larger than the mean starting size of eroded sandbars. Attrition rates of midchannel sandbars were more than double those of bank-attached sandbars, but these sandbars had starting sizes approximately half of bank-attached sandbars. The higher erosion rate of bank-attached sandbars is surprising because we would expect higher rates for midchannel bars due to their greater exposure to main channel flow and because bank-attached bars are often shielded by bank curvature or vegetated islands. We suspect that, because our erosion rates were calculated using only those bars that persisted, mean erosion rates for midchannel sandbars are potentially biased low. This is supported by the simple fact that many more bank-attached bars persisted, despite some having modest starting sizes, and higher-magnitude apparent erosion rates.

Tracking of sandbar deformation shows that erosion occurs through net along-stream shortening (Figure 12) and narrowing (Figure 13), a processes we term “streamlining,” because the physical consequence is a net decrease in perimeter and cross-stream profile of the sandbar, translating into decrease in flow resistance and contact length. Tracking of sandbar ends illustrates the relative magnitudes and mechanisms of along-stream deformation (Figure 12). Gross deformation of sandbar ends during the high-flow period shows that upstream ends of bars migrated downstream by a median of about 12% of their original length and that the downstream original sandbar ends tended to migrate upstream, but at lower magnitudes (Figure 12a). Tracking of net movement in sandbar ends during the high-flow period shows that deposition replacing erosion of the upstream end was rare, but deposition replacing erosion on the downstream end was common (Figure 12b).

During the low-flow period, about half of upstream ends did not change location, while the rest migrated downstream at much lower magnitudes than those observed during the high-flow period. Downstream ends tended to have gross upstream migration, but magnitudes tended to be low. During the low-flow period

Table 5
Seasonal Persistence and Erosion Rates of Emergent Sandbars in GS2 of the Lower Platte River Study Area, 2011 to 2012

	Bar Set No. 1[a]		Bar Set No. 2[b]	
Quantity	Midchannel[c]	Attached[c]	Midchannel[c]	Attached[c]
Survey Period No. 1 [April 2011]				
Count (*n*)	13	12	—	—
Total emergent bar area (ha)[d]	46	79	—	—
Survey Period No. 2 [July 2011]				
Count (*n*)	7	11	17	2
Total emergent bar area (ha)[d]	25	52	19	5.1
Net erosion rate (ha/day)[e]	0.2	0.2	—	—
Orig. bar area (ha)[f]	19	40	—	—
Gross erosion rate (ha/day)[g]	0.2	0.3	—	—
Survey Period No. 3 [November, 2011]				
Count (*n*)	6	11	13	2
Total emergent bar area (ha)[d]	35	67	21	5.2
Net erosion rate (ha/day)[e]	−0.11	−0.16	−0.02	0.00
Orig. bar area (ha)[f]	17	37	9.1	4.4
Gross erosion rate (ha/day)[g]	0.02	0.03	0.11	0.01
Survey Period No. 4 [April 2012]				
Count (*n*)	4	9	5	2
Total emergent bar area (ha)[d]	23	60	4.4	4.7
Net erosion rate (ha/day)[e]	0.07	0.04	0.17	0.01
Orig. bar area (ha)[f]	12	30	1.8	3.2
Gross erosion rate (ha/day)[g]	0.02	0.04	0.04	0.01
Four-season summary				
Attrition rate (% bars lost)	69%	25%	71%	0%
Mean original bar area (ha)	3.5	6.6	1.1	2.5
Mean original area of lost bars (ha)	1.8	3.3	0.8	—
Mean original area of persistent bars (ha)	7.3	7.7	1.9	2.5

[a]Set of all emergent sandbars of at least 0.8 ha in emergent area and first observed during Survey Period 1. [b] Set of all emergent sandbars of at least 0.8 ha in emergent area, and first observed during Survey Period 2. [c] Midchannel bars are sandbars free from attachment to a bank or island. Attached bars are sandbars attached to a bank or island. [d] Total area of emergent sandbars exposed above daily high water mark at time of survey. This area value includes additional deposition from intermittent pulse flows. [e] Calculated by differencing total emergent bar area from previous survey period and dividing by number of days between periods. [f] Total area remaining of emergent sandbars from first observation. This value is calculated by succesive intersection of emergent sandbar polygons in a geographic information system. This area value does not include additional deposition from intermittent pulse flows. [g] Rate of loss of original emergent sandbar area. This estimation does not include additional deposition from intermittent pulse flows between observations. ha = hectares

net erosion of sandbar ends tended to be balanced by deposition for about half of the tracked sandbars (Figure 12d). It should be noted that deposition reported here is only apparent because slight decreases in stage occurred for each successive survey, and thus, any deposition offsetting erosion occurred at a lower level than the original sandbar top-surface. This process is important because it highlights the bulk effect of sandbar deformation on bar top-surface topography, whereby the original sandbar top surface is progressively lowered as the sandbar deforms. This is the same process described in the formation of a "compound" sandbar (Bridge, 1993).

Tracking of widths indicated that sandbars tended to narrow in successive surveys but lateral attachment of unit bars offset some narrowing (Figure 13). Gross narrowing of the emergent sandbars from Sample Set 1 shows that much of the narrowing occurred during the high-flow period between April and July 2011, after which gross narrowing persisted at a relatively constant rate of about 0.1% of channel width per month. Gross narrowing during the high-flow period resulted in about a 50% decrease in sandbar width for most

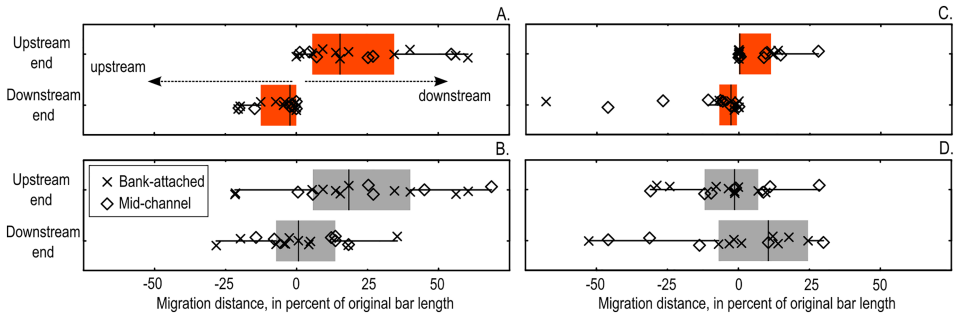

Figure 12. Box-and-whisker plots showing magnitudes of along-stream deformation of emergent sandbar lengths under high-flow and low-flow conditions: (a) Gross deformation of original sandbar area under high-flow conditions (April to July 2011). (b) Gross deformation of original sandbar length under low-flow conditions (July 2011 through April 2012). (C) came as (a) but showing net deformation. (d) Same as (b) but showing net deformation.

bars from Set 1. Gross narrowing in Sandbar Set 2 had a relatively constant rate across the low-flow period from July 2011 to April 2012. The faster rate of gross narrowing in Sandbar Set 2 during the low-flow season was likely a consequence of either (1) most sandbars in Set 2 being midchannel, and thus subject to erosion on both sides, or (2) most sandbars in Set 1 being remnants from the flood of July 2010, and thus having experienced some streamlining prior to their first survey.

The effect of streamlining is apparent in Figure 14, which shows gross changes in original sandbar area since the first observation. The gross decrease in original sandbar area is reasonably approximated by the exponential decay data model, with medians of decay constants (λ) varying from 0.002 for bank-attached sandbars, up to 0.009 for midchannel sandbars indicating mean lifetimes ($1/\lambda$) of about 100 to 500 days. Simulated posterior credible intervals for λ include 0 for set 1, indicating potential large uncertainty on median estimates of λ. However, much of this uncertainty is probably due to the small sample size. Nonetheless, posterior simulated distributions indicate 87% and 93% probability that λ is on the order of -10^{-3} for bank-attached and midchannel sandbars, respectively. Likewise, posterior distributions for Set 2 indicate 100% and 95% probability that λ is on the order of -10^{-3} for bank-attached and midchannel sandbars, respectively.

Although a direct comparison cannot be made because of potential methodological differences, values of λ for the Platte River are of similar magnitude to published values for dammed reaches of the Missouri River (Buenau et al., 2014). Midchannel sandbars had the highest decay rates, with the smaller sandbars formed

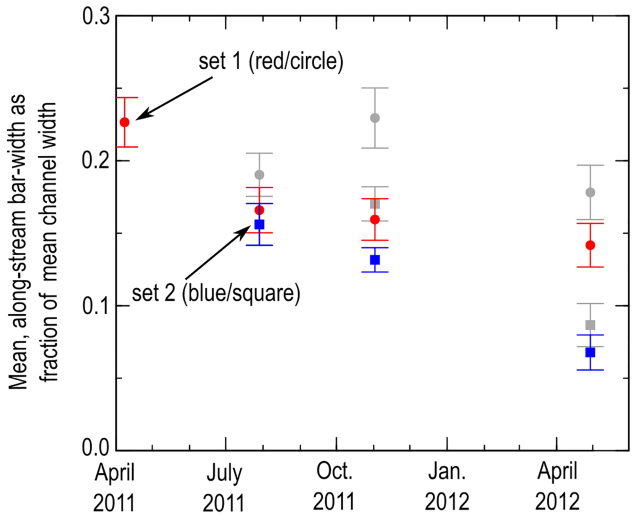

Figure 13. Scatter plots showing deformation of emergent sandbar width for two sets of sandbars. The circle points track a set of sandbars originally surveyed in April 2011, while the square points track a set of sandbars originally surveyed in July 2011. Colored points show gross changes in sandbar width, gray points show net changes in sandbar width.

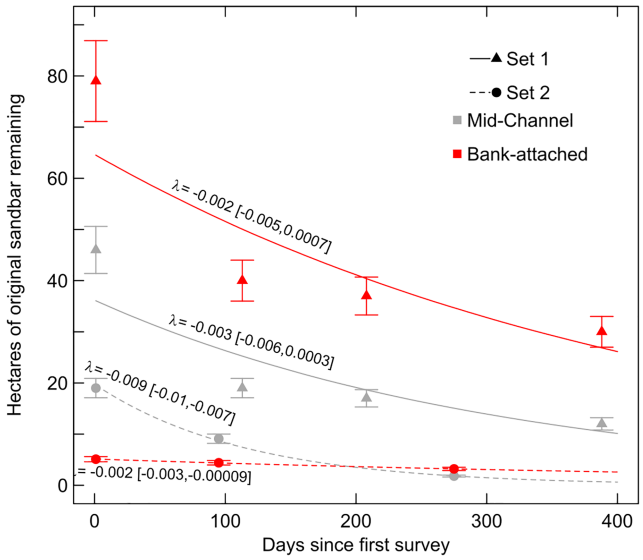

Figure 14. Time series showing changes in original sandbar area for two sample sets of sandbars tracked from 2011 to 2012. Lines are exponential fits, with the Bayesian posterior estimated median decay rate, λ, shown above each line in units of hectares per day and the Bayesian posterior estimation of the 95% credible interval of λ in brackets. Sample set 1 was formed by a 20-year return flood in the summer of 2010, and tracking of the set began in April 2011. Sample Set 2 was formed by a 2-year return flood in the spring of 2011, and tracking of the set began in July 2011. Error bars assume the 10% measurement error demonstrated by Alexander et al. (2013).

by the spring flood of 2011 having a decay rate 3 times greater than the much larger remnant midchannel sandbars formed by the flood of 2010. As mentioned above, the lower decay rate of Set 1 midchannel sandbars may be due to streamlining prior to the first measurement.

4. Discussion

4.1. Discussion Part 1: Deposition Potential of Sandbars

Values of θ near 0.5 indicate that, at reach lengths of approximately one mean channel width, every reach has equal probability of having emergent sand area greater than the segment mean; that is, ESH conditions are diffuse (nondiscrete). We interpret the spatial-temporal mean θ values of 0.43 for the study area to indicate that ESH conditions in the study area are weakly discrete. This interpretation is illustrated in the response of θ to changes in the explanatory variables and various flow conditions. Conditions following the large flood of 2010 decreased θ by a magnitude equivalent to a standard deviation decrease in ε^*, pushing ESH deposition toward more discrete conditions, whereas the small-flood in 2006 pushed θ toward more diffuse conditions. The mean value of 0.43 for θ also suggests that reaches with extensive emergent sand are somewhat common in the LPR, a finding supported by previous work (Kirsch, 1996).

Discrete expanses of large sandbars are indicative of morphologic forcing, whereby wider or expanding reaches accumulate bed material exported from contracting or narrow reaches (Repetto et al., 2002; Szupiany et al., 2012; Wu & Yeh, 2005). Alternatively, the conditions after the small flood in 2006 demonstrate that, when channel hydraulics are less influenced by the broader channel morphology, bar deposition is spatially diffuse. Distributions of θ values for reaches with nests also support variations between discrete and diffuse conditions. Ambient conditions in 2010 and 2014 tended toward more discrete expanses of ESH, while conditions where nests were located had higher potential of containing expanses of ESH than ambient conditions. By contrast, the channel conditions in 2006, particularly conditions in GS1, indicated that reaches with nests tended had θ values similar to ambient conditions. These findings are broadly supported by other studies, which have found that terns tend to nest in reaches that are wider than the segment mean (Elliott et al., 2009; Jorgensen et al., 2012) because, on a per unit discharge basis, very wide reaches would have larger values of ε^* and P^*.

The use of θ to assess potential human-induced impacts on ESH must be done considering the impact scale and ESH dynamics. At the segment-scale, equation (1) would indicate that decreases in peak flood magnitudes from planned dams or diversions might cause segment mean values of ε^* and thus θ to increase.

However, observations demonstrate declines in θ associated with large floods are caused by deposition of large, high sandbars in discrete locations. Figure 8 shows that birds tend to nest in reaches where these sandbars are more likely to be present (Figure 8). Thus, increases in segment-scale θ from decreases in peak flood magnitude would be caused by diffuse deposition of small, low sandbars, which are known to provide lower-quality nesting habitat. At the reach-scale, the impact of a change in channel morphology associated with development (i.e., bridge and levee) would be assessed by comparing changes in local θ values to the segment mean θ over a range of relevant flood frequencies. If the expected change indicates a decrease in local θ relative to the segment mean θ, the impact would be interpreted as causing a decline in ESH potential. Such impacts could be mitigated by increasing local θ elsewhere in a segment.

4.2. Discussion Part 2: Emergent Sandbar Top-Surface Flow-Response Dynamics

The collective findings of our on-the-ground surveys show that discretization of ESH happens when large floods sequester large volumes of sediment into very large sandbars. Spatially averaged sandbar top elevations from the large flood of 2010 were as much as 0.5 m higher than those deposited by the more common return floods of 2011 and 2014. Likewise, mean planimetric areas of sandbars from the 2010 flood were 3 times larger than those from the 2011 flood, and this comparison is conservative because we surveyed sandbars from this flood in April 2011 (the areas were surely larger immediately after deposition). Given the mean height of 0.95 m, and total emergent area, approximately 10^7 Mg of sediment was in sandbars in GS1 (above the stage of mean annual flow) in April 2011, or roughly 10% of the total annual sediment load at the mouth of the LPR (Heimann, 2016). The flood of 2011 reduced 2010 sandbar heights by an average of about 15 cm, resulting in a net decrease of about 460,000 Mg. By comparison, new sandbars formed by the moderate flood of 2011, sequestered only about 10^5 Mg.

Assumptions of emergent sandbar top-surface height have been controversial because of their importance in prediction of nest inundation (Catlin et al., 2010; Farnsworth et al., 2017; Jorgensen, 2009). Our findings stress the importance of accounting for changes sandbar top-surface height with formative flood magnitude. Relative to a constant depositional gap model, our bar-height growth model indicates that predictions of inundation potential should decrease for more frequent flood return periods and increase for lower frequency return periods. While our bar-height model is an improvement over simply assuming a constant depositional gap, a more general model is needed for application across the range of physical conditions in sandy-braided rivers on Earth.

Because of the importance of sandbar height in nest inundation predictions, more work is also needed to understand if the mean predicted sandbar height is representative of species nest heights. Terns, for example, have been shown to select for higher sandbars within a population of sandbars (Smith & Renken, 1991; Ziewitz et al., 1992) and higher locations within a sandbar's topography (Alexander et al., 2013; Ziewitz et al., 1992). The use of any bar height model to predict nest inundation should thus consider species-specific choice of nest location within the topographic distribution of a population of sandbars.

4.3. Discussion Part 3: Emergent Sandbar Erosion Dynamics

Data on sandbar size and persistence demonstrate the important and lasting effects of large floods on ESH in sandy-braided river systems, whereby sediment sequestered in large sandbars created during large floods disperses over several years. These large sandbars remain mostly within the same reach despite deformation during subsequent floods. These large bars also remain relatively barren, likely because their height relative to baseflow stage limits porewater available to vegetation establishing on the top surface (Amlin & Rood, 2002). The combination of size, height, and sparse vegetation of the large sandbars formed in 2010 suggests that these sandbars provided high-quality ESH for years following deposition.

Alternatively, the high rates of attrition, potential for vegetation establishment, and lower top-surface height of sandbars formed by more frequent floods, indicates that this ESH may only be viable within the year of formation. This finding hints at a physical linkage between large floods and high rates of site fidelity among successful breeding pairs of birds, which use ESH for nesting (Friedrich et al., 2014) and demonstrates the potential of large floods to influence metapopulations of birds by substantially altering the extent and quality of ESH across a landscape (Catlin et al., 2016). The large, rare flood in the lower Missouri River in 2011, for example, produced very large, natural emergent sandbars in the unchannelized reach below Gavins Point Dam (Sweeney et al., 2019). The sandbars increased tern and plover reproduction in the years after the flood (Hunt et al., 2017; Nefas et al., 2018).

4.4. Broader Implications of Findings

Although our models and observations are most applicable to the LPR, the general lessons are relevant to sandy-braided rivers worldwide. The predictor variables and structure of logistic model are widely applicable to decision-making anywhere along-stream developments may impact to ESH. Our bar-height model better reflects observations in nature than previous models, and, although a more general model is needed, the demonstration of the divergent growth of the depositional gap should help inform future efforts to predict ESH inundation. Finally, our observations of bar erosion stress the importance of large floods (>3-year R.I.) in creating high-quality, lasting ESH. This important role should be considered when planning so-called "free river" or "skimming" diversions, which often identify more frequent flood magnitudes as the most important "channel-forming" flows in sandy-braided rivers (Roy & Sinha, 2014).

Sandbar flow-response data presented here are also applicable to the broader community of geoscientists. The height of large-scale cross bedding in outcrop, interpreted to be the slip face of transverse or point bars, has been widely used as a measure of paleoflow depth (Hajek & Heller, 2012). Although our measurements did not include slip face bottoms, coupling between sandbar top-surface height and discharge (Figure 9) shows that the depositional gap may be as much as 1.5 m for large floods, indicating potential for substantial error in paleodepth estimations. Alternatively, erosion dynamics of large sandbars lends support to recently proposed methods which use migration lengths of cross bedding exposed in outcrop to differentiate between braided and meandering river patterns in the ancient (Greenberg & Hajek, 2017). Large sandbars deposited by the flood of 2010 shortened by as much as 50% by subsequent, lower-magnitude floods, providing evidence that migration lengths of braid bars would be expected to be shorter than those of point bars.

5. Summary and Conclusions

Emergent sandbar habitat (ESH) is a crucial yet poorly understood habitat element in braided rivers. We present a case study of deposition and erosion dynamics of ESH on the Lower Platte River, eastern Nebraska. The study develops linkages between hypothesized physical controls and dynamics of ESH in a braided river with mostly natural flow and sediment transport regimes. Logistic regression indicates potential for presence of large expanses of ESH (θ) was positively related to Parker (1976) stability criterion and a positive along-stream gradient in sediment transport mode and negatively related to presence of within-channel vegetation. Values of θ were also strongly influenced by hydrologic conditions in the river, whereby ambient conditions after a very large flood decreased values of θ, indicating tendency toward discrete deposition of large sandbars, and ambient conditions following a small-flood event increased values of θ, indicating a tendency toward diffuse ESH conditions. The logistic model could be used as a management decision tool by assessing changes in θ for hypothetical alterations to channel morphology or flood hydrology.

On-the-ground surveys of ESH top-surface elevation, taken after floods varying in magnitude from 1- to 20-year recurrence interval (R.I.), demonstrate a direct, positive coupling between the sandbar top-surface height and formative flood magnitude. We use the term "depositional gap" in reference to the difference in height between ESH top-surface and stage of the formative flood magnitude. Our data show an increase in the depositional gap with increasing formative flood magnitude, as well as an increase in the range of sandbar top-surface elevation, suggesting caution in using a constant, mean value in assessing probability of bird nest inundation. The growth of the depositional gap also suggests potential for errors when using large-scale cross bedding exposed in outcrop for estimating paleodepth.

Finally, we tracked ESH erosion and persistence across a full year to examine how sandbar size and channel discharge influence the extent of ESH remaining from one nesting season to the next. Our data indicate order-of-magnitude differences in ESH erosion rate for high-flow periods and low-flow periods, but ESH persistence is mostly a function of the starting size of the sandbar. Very large sandbars created by a ~20-year R.I. flood in 2010 sequestered $\sim 10^6$ Mt of sediment, which released over a period of more than 2 years. Attrition rates over the year of tracking varied from about 70% for midchannel sandbars to 25% for bars attached to a bank or vegetated island, but most of these losses occurred during the high-flow period in the spring of 2011. Alternatively, midchannel sandbars created by the 2-year R.I. flood in the spring of 2011 had much smaller starting sizes and had a 70% attrition rate during a low-flow period from July 2011 to April 2012. These data demonstrate the influence of large floods in determining the quality and extent ESH on the landscape. The high, barren, and very large sandbars created by the large 2010 flood provided high-quality

ESH for at least three seasons (summers 2010, 2011, and 2012), whereas most of the lower-quality ESH formed by the smaller flood of 2011, was gone by the spring of 2012.

Acknowledgments
The work presented here was supported through a Nebraska Environmental Trust Grant awarded to the lower Platte River Corridor Alliance, as well as contributions from lower Platte South Natural Resources District, the U.S. Geological Survey-Nebraska Water Science Center, and the University of Wyoming School of Energy Resources. The authors would like to thank the many individuals who assisted with the extensive fieldwork, in particular Chevelle Schreiner. Comments by Jason Farnsworth and two anonymous reviewers substantially improved the original manuscript. Data used in the analyses described herein can be found online (https://doi.org/10.5066/F77S7MZC). Any use of trade, firm, or product names is for descriptive purposes only and does not imply endorsement by the U.S. Government.

References

Alexander, J. S., & Densmore, B. K. (2019). Orthophotography classification and ground surveys to understand sandbar formation, geometry, and persistence in the lower Platte River in Nebraska, 2006–2014. U.S. Geological Survey data release. https://doi.org/10.5066/F77S7MZC

Alexander, J. S., Schultze, D. M., & Zelt, R. B. (2013). Emergent sandbar dynamics in the lower Platte River in eastern Nebraska: Methods and results of pilot study. 2011: U.S. Geological Survey Scientific Investigations Report 2013–5031, 42 p.

Amlin, N. M., & Rood, S. B. (2002). Comparative tolerances of riparian willows and cottonwoods to water-table decline. *Wetlands*, *22*(2), 338–346.

Ashmore, P. E. (1996). Mid-channel bar growth and its relationship to local flow strength and direction. *Earth Surface Processes and Landforms*, *21*(2), 103–123.

Ashworth, P. J., Best, J. L., Roden, J. E., Bristow, C. S., & Klaassen, G. J. (2000). Morphological evolution and dynamics of a large, sand braid-bar, Jamuna River, Bangladesh. *Sedimentology*, *47*(3), 533–555.

Bentall, R. (1991). Facts and figures about Nebraska Rivers. Conservation and Survey Division.

Bentall, R., & Schaffer, F. B. (1979). Availability and use of water in Nebraska, 1975. Nebraska Water Supply Paper Number 48 June 1979. 121 P, 27 Fig.

Brice, J. C. (1964). Channel patterns and terraces of the Loup Rivers in Nebraska: U.S.Geological Survey Professional Paper 422-D, 41 p.

Bridge, J. S. (1993). The interaction between channel geometry, water flow, sediment transport and deposition in braided rivers. *Geological Society, London, Special Publications*, *75*(1), 13–71.

Buchanan, J., & Schumm, S. A. (1990). The riverscape—Niobrara River. *Surface Water Hydrology*, *1*, 314–321.

Buenau, K. E., Hiller, T. L., & Tyre, A. J. (2014). Modelling the effects of river flow on population dynamics of piping plovers, (charadrius Melodus) and Least Terns, (sternula Antillarum) nesting on the Missouri River. *River Research and Applications*, *30*(8), 964–975.

Cant, D. J., & Walker, R. G. (1978). Fluvial processes and facies sequences in the sandy braided South Saskatchewan River, Canada. *Sedimentology*, *25*(5), 625–648.

Catlin, D., Jacobson, R., Sherfy, M., Anteau, M., Felio, J., Fraser, J., & Stucker, J. (2010). Discussion of "Natural hydrograph of the Missouri River near Sioux City and the least tern and piping plover" by Donald G. Jorgensen. *Journal of Hydrologic Engineering*, *15*(12), 1076–1078.

Catlin, D. H., Milenkaya, O., Hunt, K. L., Friedrich, M. J., & Fraser, J. D. (2014). Can river management improve the piping plover's long-term survival on the Missouri River? *Biological Conservation*, *180*(Supplement C), 196–205.

Catlin, D. H., Zeigler, S. L., Brown, M. B., Dinan, L. R., Fraser, J. D., Hunt, K. L., & Jorgensen, J. G. (2016). Metapopulation viability of an endangered shorebird depends on dispersal and human-created habitats: Piping plovers, (Charadrius melodus) and prairie rivers. *Movement Ecology*, *4*, 6.

Church, M., & Ferguson, R. I. (2015). Morphodynamics: Rivers beyond steady state. *Water Resources Research*, *51*, 1883–1897.

Coleman, J. M. (1969). Brahmaputra river: Channel processes and sedimentation. *Sedimentary Geology*, *3*(2), 129–239.

Collinson, J. D. (1970). Bedforms of the Tana River, Norway. *Geografiska Annaler. Series A, Physical Geography*, *52*(1), 31–56.

Council, N. R. (2002). The Missouri River ecosystem: Exploring the prospects for recovery.

Council, N. R. (2004). Endangered and threatened species of the Platte River.

Council, N. R. (2010). Missouri River planning: Recognizing and incorporating sediment management.

Crowley, K. D. (1983). Large-scale bed configurations (macroforms) Platte River Basin, Colorado and Nebraska: Primary structures and formative processes. *GSA Bulletin*, *94*(1), 117–133.

Dietrich, W. E., & Smith, J. D. (1983). Influence of the point bar on flow through curved channels. *Water Resources Research*, *19*(5), 1173–1192.

Dilawar, M., & Sharma, V. (2016). A new breeding location of Indian Skimmer Rynchops albicollis, and notes on other birds in Son Gharial Wildlife Sanctuary, Madhya Pradesh India. *Indian Birds*, *11*(2), 35–38.

Dilbone, E., Legleiter, C. J., Alexander, J. S., & McElroy, B. (2018). Spectrally based bathymetric mapping of a dynamic, sand-bedded channel: Niobrara River, Nebraska USA. *River Research and Applications*, *34*(5), 430–441.

Dixon, M. D. (2003). Effects of flow pattern on riparian seedling recruitment on sandbars in the Wisconsin River, Wisconsin, USA. *Wetlands*, *23*(1), 125–139.

Driesen, T. (1996). Creative management under the endangered species act: A case study of the Missouri River Terns and Plovers. *Great Plains Natural Resources Journal*, *1*, 463.

Duckworth, J. W., Timmins, R. J., & Evans, T. D. (1998). The conservation status of the river lapwing Vanellus duvaucelii in southern Laos. *Biological Conservation*, *84*(3), 215–222.

Elliott, C. M., Huhmann, B. L., & Jacobson, R. B. (2009). Geomorphic classification of the Lower Platte River, Nebraska: U.S.Geological Survey Professional Paper 2009-5198, 29 p.

Eschner, T. R., Hadley, R. F., & Crowley, K. D. (1983). Hydrologic and morphologic changes in channels of the Platte River basin in Colorado, Wyoming, and Nebraska: A historical perspective: U.S.Geological Survey Professional Paper 1277-A, 39 p.

Evans, T. D. (2001). Ornithological records from Savannakhet Province, Lao PDR, January-July 1997. Forktail 21–28.

Farnsworth, J. M., Baasch, D. M., Smith, C. B., & Werbylo, K. L. (2017). Reproductive ecology of interior least tern and piping plover in relation to Platte River hydrology and sandbar dynamics. *Ecology and Evolution*, *7*(10), 3579–3589.

Fenneman, N. M. (1928). Physiographic divisions of the United States. Annals of the Association of American Geographers, *18*(4), 261–353.

Friedman, J. M., Osterkamp, W. R., Scott, M. L., & Auble, G. T. (1998). Downstream effects of dams on channel geometry and bottomland vegetation: Regional patterns in the Great Plains. *Wetlands*, *18*(4), 619–633.

Friedrich, M. J., Hunt, K. L., Catlin, D. H., & Fraser, J. D. (2014). The importance of site to mate choice: Mate and site fidelity in Piping Plovers. *The Auk*, *132*(1), 265–276.

Gimenes, M., & Anjos, L. dos. (2004). Bird richness on the islands of the Upper Paraná River, Paraná and Mato Grosso do Sul border, Brazil. *Structure and Functioning of the Paraná River and Its Floodplain-LTER-Site*, *6*, 203–207.

Ginting, D., Zelt, R. B., & Linard, J. I. (2007). Temporal differences in the hydrologic regime of the Lower Platte River, Nebraska, 1895–2006. U.S. Geological Survey Scientific Investigations Report 2007-5267, 43 p.

Greenberg, E. B., & Hajek, E. A. (2017). Reconstructing fluvial channel mobility through the Paleocene–Eocene Thermal Maximum. In 11^{th} *International Conference on Fluvial Sedimentology. Program with abstracts*.

Hajek, E. A., & Heller, P. L. (2012). Flow-depth scaling in alluvial architecture and nonmarine sequence stratigraphy: Example from the Castlegate Sandstone, Central Utah, U.S.A. *Journal of Sedimentary Research*, *82*(2), 121–130.
Heimann, D. C. (2016). Generalized sediment budgets of the Lower Missouri River, 1968–2014. U.S. Geological Survey Scientific Investigations Report 2016-5097, 64 p.
Hunt, K. L., Fraser, J. D., Karpanty, S. M., & Catlin, D. H. (2017). Body condition of piping plovers (Charadrius melodus) and prey abundance on flood-created habitat on the Missouri River, USA. *The Wilson Journal of Ornithology*, *129*(4), 754–764.
Jiongxin, X. (1997). Evolution of mid-channel bars in a braided river and complex response to reservoir construction: An example from the middle Hanjiang River, China. *Earth Surface Processes and Landforms*, *22*(10), 953–965.
Joeckel, R. M., & Henebry, G. M. (2008). Channel and island change in the lower Platte River, Eastern Nebraska, USA: 1855–2005. *Geomorphology*, *102*(3), 407–418.
Johnson, W. C. (1994). Woodland expansions in the Platte River, Nebraska: Patterns and Causes. *Ecological Monographs*, *64*(1), 45–84.
Jorgensen, D. G. (2009). Natural hydrograph of the Missouri River near Sioux City and the least tern and piping plover. *Journal of Hydrologic Engineering*, *14*(12), 1365–1373.
Jorgensen, J., Brown, M., & Tyre, A. (2012). Channel width and least tern and piping plover nesting incidence on the lower Platte River, Nebraska. *Great Plains Research*, *22*(1), 59–67.
Kennedy, E. J. (1984). Discharge ratings at gaging stations. U.S. Geological Survey Techniques of Water-Resources Investigations of the United States Geological Survey 3-A10, 59 p.
Kinzel, P. J., & Runge, J. T. (2010). Summary of bed-sediment measurements along the Platte River, Nebraska, 1931-2009. U.S. Geological Survey Fact Sheet 2010-3087, 4 p.
Kirsch, E. M. (1996). *Habitat selection and productivity of least terns on the Lower Platte River, Nebraska*, Wildlife Monographs (Vol. 132, pp. 3–48).
Kleinhans, M. G. (2010). Sorting out river channel patterns. *Progress in Physical Geography*, *34*(3), 287–326.
Leopold, L. B., & Wolman, M. G. (1957). River channel patterns: Braided, meandering, and straight (USGS Numbered Series No. 282-B) p. 50, Washington, D.C.U.S. Government Printing Office.
Lott, C. A., Wiley, R. L., Fischer, R. A., Hartfield, P. D., & Scott, J. M. (2013). Interior least tern (Sternula antillarum) breeding distribution and ecology: Implications for population-level studies and the evaluation of alternative management strategies on large, regulated rivers. *Ecology and Evolution*, *3*(10), 3613–3627.
Mohrig, D. (1994). Spatial evolution of dunes in a sandy river (PhD Dissertation), University of Washington, Seattle. 119 p.
Nefas, S. M., Hunt, K. L., Fraser, J. D., Karpanty, S. M., & Catlin, D. H. (2018). Least tern (Sternula antillarum) nest success and chick survival on the Missouri River following historic flooding. *The Wilson Journal of Ornithology*, *130*(2), 371–376.
Nicholas, A. P. (2013). Modelling the continuum of river channel patterns. *Earth Surface Processes and Landforms*, *38*(10), 1187–1196.
Parker, G. (1976). On the cause and characteristic scales of meandering and braiding in rivers. *Journal of Fluid Mechanics*, *76*(3), 457–480.
Parker, N. O., Sambrook Smith, G. H., Ashworth, P. J., Best, J. L., Lane, S. N., Lunt, I. A., et al. (2013). Quantification of the relation between surface morphodynamics and subsurface sedimentological product in sandy braided rivers. *Sedimentology*, *60*(3), 820–839.
Platte River Recovery Program (2015). Data synthesis compilation: Interior least tern (Sterna antillarum) and piping plover (Charadrius melodus) habitat synthesis chapters. Executive Director's Office of the Platte River Recovery program, Kearney, Nebraska. Available from https://platteriverprogram.org/ (Accessed 1 May 2019).
Plummer, M., Stukalov, A., & Denwood, M. (2016). rjags: Bayesian graphical models using MCMC (R Package Version, 4-6).
Price, K. H., & Martz, M. (2007). Evaluating constructed backwater habitat and sandbar islands on the Missouri River. World Environmental and Water Resources Congress 2007.
R Core Team (2017). A language and environment for statistical computing. R Foundation for Statistical Computing, Vienna, Austria. URL https://www.R-project.org/
Repetto, R., Tubino, M., & Paola, C. (2002). Planimetric instability of channels with variable width. *Journal of Fluid Mechanics*, *457*, 79–109.
Rhoads, B. L., & Welford, M. R. (1991). Initiation of river meandering. *Progress in Physical Geography*, *15*(2), 127–156.
Rosenberg, G. H. (1990). Habitat specialization and foraging behavior by birds of Amazonian River Islands in Northeastern Peru. *The Condor*, *92*(2), 427–443.
Rouse, H. (1939). Experiments on the mechanics of sediment suspension. In Proceedings of the Fifth International Congress for Applied Mechanics (pp. 550–554) New York: John Wiley and Sons.
Roy, N. G., & Sinha, R. (2014). Effective discharge for suspended sediment transport of the Ganga River and its geomorphic implication. *Geomorphology*, *227*, 18–30.
Sambrook Smith, G. H., Ashworth, P. J., Best, J. L., Lunt, I. A., Orfeo, O., & Parsons, D. L. (2009). The sedimentology and alluvial architecture of a large braid bar, Río Paraná, Argentina. *Journal of Sedimentary Research*, *79*(8), 29–642.
Santos, M. L., & Stevaux, J. C. (2000). Facies and architectural analysis of channel sandy macroforms in the upper Parana river. *Quaternary International*, *72*(1), 87–94.
Sarma, J. N. (2005). Fluvial process and morphology of the Brahmaputra River in Assam, India. *Geomorphology*, *70*(3), 226–256.
Schuurman, F., Marra, W. A., & Kleinhans, M. G. (2013). Physics-based modeling of large braided sand-bed rivers: Bar pattern formation, dynamics, and sensitivity. *Journal of Geophysical Research: Earth Surface*, *118*, 2509–2527. https://doi.org/10.1002/2013JF002896
Schwilk, J. A., & Claassen, A. H. (2012). Evidence of the Mekong River as a migratory corridor for shorebirds, including the first record of slender-billed gull Chroicocephalus genei for Cambodia. *Cambodian Journal of Natural History*, *2012*(2), 111–114.
Smith, N. D. (1971). Transverse bars and braiding in the Lower Platte River, Nebraska. *GSA Bulletin*, *82*(12), 3407–3420.
Smith, J. W., & Renken, R. B. (1991). Least tern nesting habitat in the Mississippi River Valley adjacent to Missouri. *Journal of Field Ornithology*, *62*(4), 497–504.
Smith, J. W., & Renken, R. B. (1993). Reproductive success of least terns in the Mississippi River Valley. *Colonial Waterbirds*, *16*(1), 39–44.
Struiksma, N., Olesen, K. W., Flokstra, C., & Vriend, D. H. J. D. (1985). Bed deformation in curved alluvial channels. *Journal of Hydraulic Research*, *23*(1), 57–79.
Sundar, K. G. (2004). Observations on breeding Indian Skimmers Rynchops albicollis in the National Chambal Sanctuary, Uttar Pradesh, India. *Forktail*, *20*, 89–90.
Sweeney, M. R., Fischer, B., Wermers, K., & Cowman, T. (2019). Eolian and fluvial modification of Missouri River sandbars deposited by the 2011 flood, USA. *Geomorphology*, *327*, 111–125.
Szupiany, R. N., Amsler, M. L., Hernandez, J., Parsons, D. R., Best, J. L., Fornari, E., & Trento, A. (2012). Flow fields, bed shear stresses, and suspended bed sediment dynamics in bifurcations of a large river. *Water Resources Research*, *48*, W11515. https://doi.org/10.1029/2011WR011677
Tal, M., & Paola, C. (2007). Dynamic single-thread channels maintained by the interaction of flow and vegetation. *Geology*, *35*(4), 347–350.

Taylor, J. (1996). Introduction to error analysis, the study of uncertainties in physical measurements.
Tracy-Smith, E., Galat, D. L., & Jacobson, R. B. (2012). Effects of flow dynamics on the aquatic-terrestrial transition zone (ATTZ) of Lower Missouri River Sandbars with implications for selected biota. *River Research and Applications*, *28*(7), 793–813.
U.S. Army Corps of Engineers (2014). Lower Platte River Cumulative Impact Study—Phase III Summary Report. Omaha District, 55 p.
Valenzuela, N. (2001). Maternal effects on life-history traits in the Amazonian Giant River Turtle Podocnemis expansa. *Journal of Herpetology*, *35*(3), 368–378.
Whitaker, R. (2007). The Gharial: Going extinct again. *Iguana*, *14*(1), 25–32.
Williams, G. P. (1978). The case of the shrinking channels; the North Platte and Platte rivers in Nebraska. U.S. Geological Survey Professional Paper 781, 48 p.
Wright, S., & Parker, G. (2004). Flow resistance and suspended load in sand-bed rivers: Simplified stratification model. *Journal of Hydraulic Engineering*, *130*(8), 796–805.
Wu, F. C., Shao, Y. C., Chen, Y. C., & Journal of Geophysical Research (2011). Quantifying the forcing effect of channel width variations on free bars: Morphodynamic modeling based on characteristic dissipative Galerkin scheme, *116*, F03023. https://doi.org/10.1029/2010JF001941
Wu, F. C., & Yeh, T. H. (2005). Forced bars induced by variations of channel width: Implications for incipient bifurcation. *Journal of Geophysical Research*, *110*, F02009. https://doi.org/10.1029/2004JF000160
Ziewitz, J. W., Sidle, J. G., & Dinan, J. J. (1992). Habitat conservation for nesting least terns and piping plovers on the Platte River, Nebraska. *Prairie Naturalist*, *24*(1), 1–20.